

# Microensing optical depth toward the Galactic Bulge using bright sources from OGLE-II

T. Sumi<sup>1</sup>, P. R. Woźniak<sup>2</sup>, A. Udalski<sup>3</sup>, M. Szymański<sup>3</sup>, M. Kubiak<sup>3</sup>, G. Pietrzyński<sup>3,4</sup>,  
I. Soszyński<sup>3,4</sup>, K. Żebruń<sup>3</sup>, O. Szewczyk<sup>3</sup>, Ł. Wyrzykowski<sup>3</sup> & B. Paczyński<sup>1</sup>

## ABSTRACT

We present a measurement of the microlensing optical depth toward the Galactic Bulge based on 4 years of the OGLE-II survey. We consider only bright sources in the extended Red Clump Giant (RCG) region of the Color-Magnitude Diagram, in 20 bulge fields covering  $\sim 5 \text{ deg}^2$  between  $0^\circ < l < 3^\circ$  and  $-4^\circ < b < -2^\circ$ . Using a sample of 32 events we find  $\tau = 2.55_{-0.46}^{+0.57} \times 10^{-6}$  at  $(l, b) = (1.^\circ 16, -2.^\circ 75)$ . Taking into account the measured gradient along the Galactic latitude  $b$ ,  $\tau = [(4.48 \pm 2.37) + (0.78 \pm 0.84) \times b] \times 10^{-6}$ , this value is consistent with previous measurements using RCG sources and recent theoretical predictions. We determine the microlensing parameters and select events using a model light curve that allows for flux blending. Photometric quality delivered by Difference Image Analysis (DIA) combined with the  $1.3''$  median seeing of the OGLE-II images are sufficient to constrain and reject the majority of strong blends. We find that  $\sim 38\%$  of the OGLE-II events which appear to have RCG sources are actually due to much fainter stars blended with a bright companion. We show explicitly that model fits without blending result in similar  $\tau$  estimates through partial cancellation of contributions from higher detection efficiency, underestimated time-scales and larger number of selected events. The near cancellation of the optical depth bias and the fact that microlensing event selection based on models without blending discriminates against blends have been utilized by previous analyses based on RCG sources. The latter approach, however, leads to biased time-scale distributions and event rates. Consequently,

---

<sup>1</sup>Princeton University Observatory, Princeton, NJ 08544-1001, USA,  
e-mail: (sumi, bp)@astro.princeton.edu

<sup>2</sup>Los Alamos National Laboratory, MS-D466, Los Alamos, NM 87545,  
e-mail: woźniak@lanl.gov

<sup>3</sup>Warsaw University Observatory, Al. Ujazdowskie 4, 00-478 Warszawa, Poland,  
e-mail: (udalski, msz, mk, pietrzyn, soszynsk, zebrun, szewczyk, wyrzykow)@astrouw.edu.pl

<sup>4</sup>Universidad de Concepción, Departamento de Física, Casilla 160-C, Concepción, Chile

microlensing studies should carefully consider source confusion effects even for bright stars.

*Subject headings:* gravitational lensing – Galaxy: bulge – stars: variables: other

## 1. Introduction

Following the suggestion of Paczyński (1991) and Griest et al. (1991) several teams have carried out microlensing surveys toward the Galactic Bulge (GB). To date, well over  $2 \times 10^3$  microlensing events in the GB have been detected by those groups: OGLE (Udalski et al. 1994, 2000; Woźniak et al. 2001; Udalski 2003), MOA (Bond et al. 2001; Sumi et al. 2003), MACHO (Alcock et al. 1997, 2000b) and EROS (Afonso et al. 2003). Thousands of detections are expected in the upcoming years from MOA<sup>1</sup> and OGLE-III<sup>2</sup>. It is now well understood that these observations are useful for studying the structure, kinematics and dynamics of the Galaxy, and the stellar mass function, as the event rate and time-scale distributions are related to the masses and velocities of lens objects.

The magnification of a microlensing event is described by (Paczynski 1986)

$$A(u) = \frac{u^2 + 2}{u\sqrt{u^2 + 4}}, \quad (1)$$

where  $u$  is the projected separation of the source and lens in units of the Einstein radius  $R_E$  which is given by

$$R_E(M, x) = \sqrt{\frac{4GM}{c^2} D_s x (1 - x)}, \quad (2)$$

where  $M$  is the lens mass,  $x = D_l/D_s$  is the normalized lens distance and  $D_l$  and  $D_s$  are the observer-lens and the observer-source distances. The time variation of  $u = u(t)$  is

$$u(t) = \sqrt{u_{\min}^2 + \left(\frac{t - t_0}{t_E}\right)^2}, \quad (3)$$

---

<sup>1</sup><http://www.massey.ac.nz/~iabond/alert/alert.html>

<sup>2</sup><http://www.astrouw.edu.pl/~ogle/ogle3/ews/ews.html>

where  $u_{\min}$ ,  $t_0$ ,  $t_E = R_E/v_t$  and  $v_t$  are, respectively, the minimum impact parameter in units of  $R_E$ , the time of maximum magnification, the event time-scale and the transverse velocity of the lens relative to the line of sight toward the source star. From light curve alone, one can determine the values of  $u_{\min}$ ,  $t_0$  and  $t_E$ , but not the values of  $M$ ,  $x$  or  $v_t$ .

Microensing optical depth (the total cross section for microensing) is directly related to the mass density of compact objects along the line of sight (Paczynski 1996). However, previous results have been controversial. Paczynski (1991) and Griest et al. (1991) first predicted the optical depth of  $\tau \sim 5 \times 10^{-7}$ , assuming that all events were associated with known disk stars. After the first several bulge events were reported by OGLE (Udalski et al. 1994), the high event rate prompted Kiraga & Paczynski (1994) to evaluate the contribution of bulge stars in addition to the disk stars. They estimated  $\tau \sim 8.5 \times 10^{-7}$  and concluded that the value could be about twice as large, if the bulge were elongated along the line of sight. Nevertheless, the first measurements of the optical depth,  $\tau \sim 3.3 \times 10^{-6}$  by OGLE (Udalski et al. 1994) and  $\tau \sim 3.9_{-1.2}^{+1.8} \times 10^{-6}$  by MACHO (Alcock et al. 1997), were well above the predictions. Recent studies based on Difference Image Analysis (DIA)—less sensitive to the systematics of blending in crowded fields—also found large optical depths:  $\tau = 3.23_{-0.50}^{+0.52} \times 10^{-6}$  at  $(l, b) = (2.^{\circ}68, -3.^{\circ}35)$  from 99 events by MACHO (Alcock et al. 2000b) and  $\tau = 3.36_{-0.81}^{+1.11} \times 10^{-6}$  at  $(l, b) = (3.^{\circ}0, -3.^{\circ}8)$  from 28 events by MOA (Sumi et al. 2003). The latter values were adjusted for the presence of the foreground disk stars, and the uncorrected measurements are considerably lower, i.e.  $\tau = 2.43_{-0.38}^{+0.39} \times 10^{-6}$  and  $\tau = 2.59_{-0.64}^{+0.84} \times 10^{-6}$ , respectively.

To explain high optical depths a number of authors have suggested the presence of a bar oriented along our line of sight to the GB (Paczynski et al. 1994; Zhao, Spergel & Rich 1995), and have adopted various values of the bar orientation and mass (Han & Gould 1995; Zhao & Mao 1996; Peale 1998; Gyuk 1999). The resulting values are in the range  $\tau = 0.8 - 2.0 \times 10^{-6}$ . Binney et al. (2000) have shown that high optical depth measurements available at the time could not be easily reconciled with our general understanding of the Galactic dynamics, and that the standard models of the Galaxy would need to be revised.

Alcock et al. (1997) raised the possibility of a systematic bias in the optical depth measurement due to the difficulties of measuring  $t_E$  associated with merging unresolved sources. When the actual source base-line flux is unknown,  $t_E$  and  $u_{\min}$  are degenerate in relatively low signal-to-noise ratio (S/N) events (c.f. Woźniak & Paczynski 1997; Han 1999; Bond et al. 2001; Gould & An 2002). Popowski et al. (2001) postulated that optical depth may be estimated without a bias due to blending by using only events with bright source stars, such as Red Clump Giants (RCG), in which blending is assumed to be negligible. Although the first measurements by Alcock et al. (1997) gave a high value

$\tau \sim 3.9_{-1.2}^{+1.8} \times 10^{-6}$ , the recent measurements based on events with RCG sources have returned lower optical depths:  $2.0 \pm 0.4 \times 10^{-6}$  at  $(l, b) = (3.^{\circ}9, -3.^{\circ}8)$  from 50 events by MACHO (Popowski et al. 2001),  $0.94 \pm 0.29 \times 10^{-6}$  at  $(l, b) = (2.^{\circ}5, -4.^{\circ}0)$  from 16 events by EROS (Afonso et al. 2003) and  $2.17_{-0.38}^{+0.47} \times 10^{-6}$  at  $(l, b) = (1.^{\circ}50, -2.^{\circ}68)$  from 42 events by MACHO (Popowski et al. 2004).

In this paper we present a measurement of the microlensing optical depth in the direction of the GB based on the full 4-year extent of the OGLE-II monitoring data. For analysis we select only high S/N events with bright apparent source stars in the RCG region. In order to better understand the systematics of this complex measurement, we proceed without assuming that blending is negligible. In the first part of the paper we present the photometric data (§ 2), selection of microlensing events (§ 3), computation of the detection efficiency (§ 4) and estimation of the optical depth (§ 5). This is followed, in the second part (§ 6 and § 7), by a description of various cross checks and general discussion. We primarily examine source confusion and the effect of reintroducing the assumption of negligible blending in our bright event sample.

## 2. Data

The data used in this analysis were collected between 1997 and 2000, during the second phase of the OGLE experiment. All observations were made with the 1.3-m Warsaw telescope located at the Las Campanas Observatory, Chile. The observatory is operated by the Carnegie Institution of Washington. The "first generation" camera has a SITe  $2048 \times 2048$  pixel CCD detector with pixel size of  $24 \mu\text{m}$  resulting in  $0.417 \text{ arcsec/pixel}$  scale. Images of the GB fields were taken in drift-scan mode at "medium" readout speed with the gain  $7.1 e^-/\text{ADU}$  and readout noise of  $6.3 e^-$ . A single  $2048 \times 8192$  pixel frame covers an area of  $0.24 \times 0.95 \text{ deg}^2$ . Saturation level is about 55,000 ADU. Details of the instrumentation setup can be found in Udalski, Kubiak & Szymański (1997).

In this paper we use *I*-band images for the 20 central OGLE-II fields in the GB. Between 138 and 555 frames were available in each field. The remaining 29 fields are either harder to model (because of a prominent disk component), or cannot be treated as co-located with the rest and averaged. The event number statistics in those fields is not sufficient for an independent determination of  $\tau$ . A reliable map of the microlensing optical depth must await the full analysis of the OGLE-III data. The centers of the analyzed fields are listed in Table 1. The time baseline of the survey is almost 4 years. There are gaps between the observing seasons when GB cannot be observed from Earth, each about 3 months long. The median seeing was  $1.3''$ . Astrometric and photometric scales are defined by multi-color maps

of Udalski et al. (2002), comprising positions and  $VI$ -band photometry of  $\sim 3 \times 10^7$  stars in all 49 GB fields. Photometric zero points are accurate to about 0.04 mag.

We adopt a hybrid approach to photometry with source detection and centroiding on reference images using DoPHOT package (Schechter, Mateo & Saha 1993), combined with the DIA photometry to lower the point-to-point scatter (Alard & Lupton 1998; Alard 2000; Woźniak 2000). A high S/N reference image for each field was taken to be a mean of 20 frames with the best overall seeing and background. To obtain a difference frame we convolve the reference image with the PSF matching kernel and subtract the result from a given survey frame, after interpolating to the same pixel grid. PSF photometry on difference frames is performed only for objects detected on the reference image using fixed positions found by DoPHOT.

### 3. Microlensing event selection

Criteria for selecting candidate microlensing events are summarized in Table 2.

#### 3.1. Defining a population of bright Galactic Bulge sources

For the optical depth analysis we select only those microlensing events that occurred in bright stars. Red Clump Giants are sufficiently numerous for acceptable counting statistics, but not too numerous. Their combined seeing disks still cover a small fraction of the survey area. Therefore, RCGs should be less affected by source confusion with stars  $\sim 2$  mag deeper in the luminosity function (LF) compared to fainter stars with higher number density. Note that by itself this does not guarantee that we can entirely neglect blending in our samples. We discuss this issue in § 3.5 and § 6.2.

Only stars with more than 70 data points are considered. In the Color Magnitude Diagram (CMD) we define the extended Red Clump Giant (RCG) region using a condition:  $I_0 < I_{\text{RC,th}}$  and  $I_0 < 9 \times (V - I)_0 + I_{\text{RC}} - 5.5$  (Fig. 1). Extinction corrected magnitudes and colors, i.e.  $I_0$  and  $(V - I)_0$ , are obtained for each star using the OGLE-II reddening map of the GB (Sumi 2004). The magnitude threshold is set at  $I_{\text{RC,th}} = I_{\text{RC}} + 1$ , where  $I_{\text{RC}}$  is the mean magnitude of the RCG population in a given field.  $I_{\text{RC}}$  is estimated according to the prescription in Sumi (2004) and accounts for the Galactic bar geometry. This procedure is very effective in rejecting most of the disk main sequence. In contrast with previous analyses using RCG sources (Afonso et al. 2003; Popowski et al. 2004), our extended RCG region includes not only RCGs, but also Red Giants and Red Supper Giants. The total number of

sources selected in all 20 fields was 1,084,267 (level 0 criteria in Table 2).

### 3.2. Searching for peaks consistent with microlensing

Level 1 criteria detect generic flux brightening in otherwise quiet objects, followed by microlensing model fitting at level 2 (Table 2). We define a "peak" as a group of consecutive data points in the light curve that includes at least 5 data points with significance  $\sigma \geq 1.6$ . At least 3 of those points should have  $\sigma \geq 3$ . Counting of consecutive data points allows for one failure, i.e.  $\sigma < 1.6$  between data points.

The baseline flux and the significance of each photometric measurement with respect to that baseline are established within a centered running window spanning 500 d. We adopted:

$$\sigma_i = \frac{F_i - F_{\text{med,out}}}{\sqrt{\sigma_{F,i}^2 + \sigma_{\text{out}}^2}}, \quad (4)$$

where  $F_i$  and  $\sigma_{F,i}$  are the flux and flux error of the  $i$ -th data point.  $F_{\text{med,out}}$  and  $\sigma_{\text{out}}^2$  are the median and variance of all data points outside the window.

There are further conditions on the number of detected peaks ( $N_{\text{peak}}$ ), the maximum significance level reached by any point in any of those peaks ( $\sigma_{\text{max}}$ ), and the integrated significance of the peak where  $\sigma_{\text{max}}$  occurred ( $\sum_{\text{peak,max}} \sigma_i$ ). Full details are in Table 2. For lower S/N peaks ( $\sigma_{\text{max}} < 10$ ) we allow less noise in the baseline and limit the reduced  $\chi^2$ :  $\chi_{\text{out}}^2/d.o.f. < 2.2$ .

The non-linear model fitting is performed using the MINUIT package (CERN Lib. 1998) which provides the best fit parameters and corresponding 68% confidence intervals (for 1 parameter of interest). We fit a single lens microlensing model in the form:

$$F(t) = F_s A(t) + F_b, \quad (5)$$

where  $A(t)$  is given in Equations 1–3,  $F_s$  and  $F_b$  are the baseline fluxes of the source star and the blended background star, respectively. Table 2 lists all requirements on the quality of the best fit model  $\chi_{\text{ml}}^2/d.o.f.$  and on the parameters. Long Period Variables and Novae in our data set tend to have unusually large  $t_E$  or  $u_{\text{min}} > 1$ . None of the 135 candidates that remain at this point are likely to be a variable star in one of those categories. In Fig. 2 we show light curves of two objects which failed the  $t_E$  cut.

### 3.3. Removing spurious events and low quality light curves

PSF photometry on difference frames is performed assuming a constant background at zero counts. The PSF matching kernel does not handle the extended wings of very bright stars due to lack of signal there. This is why light curves of some stars follow the intrinsic or seeing induced variability of their much brighter neighbors (Sumi et al. 2004b). The effect is further exacerbated by the presence of spurious objects around bright stars in DoPHOT output. Such artifacts around microlensed stars and other variables (primarily Novae) have to be rejected from the list of microlensing events. This is accomplished by cross-referencing the list of positions for our bright candidate events with an analogous list constructed for events of any brightness (both after level 0–2 selection only). In case there is a “sibling” event within 20 pixels that occurred at a similar time  $t_0 \pm 6$  d, the one with lower  $\sigma_{\max}$  is rejected from its respective list.

Most of the 54 rejected light curves are associated with a possible nova which appeared in BUL\_SC4 field around HJD=2450614.79 d. Stars as far as 100 pixels around it were affected. Several rejected artifacts are associated with microlensing events. At level 3 (Table 2) our automated criteria select 81 candidate microlensing events. All light curves in that group were also selected as microlensing events by visual inspection. Up to this point, 41 candidates flagged as microlensing by eye were rejected because of low S/N or  $u_{\min} > 1$ . Note that strongly degenerate events can fail if they happen to have the best fit model with  $u_{\min} > 1$ .

Out of the 81 remaining events, 69 have estimates of errors in all parameters from MINUIT. In practice, i.e. with any decent initial guess, the only reason for MINUIT error estimates not to converge is a very wide and shallow  $\chi^2$  surface. Events with such degenerate models have unreliable best fit parameters and are not used in the optical depth measurement (level 4, Table 2). Furthermore, we required  $\chi_{\text{ml}}^2 < 3.5$  (level 5 selection in Table 2). This rejects three events with a low amplitude variability visible in the baseline and caused by the nearby bright variable stars or by differential refraction. The requirement on the goodness of fit prevents such variability from distorting the parameters of the fitted model.

### 3.4. Exotic microlensing events

Two binary lens events are rejected by the  $\chi_{\text{ml}}^2$  cut from the previous paragraph. Some binary microlensing events show only weak deviations with respect to the basic case. The detectability of such events is sensitive to the details of the temporal sampling and coverage. The deviations that were missed may still significantly distort the results of the single lens model fitting. We cross-referenced our event sample with other published samples from

MACHO (Alcock et al. 2000a; Thomas et al. 2004), MOA (Sumi et al. 2003), EROS (Afonso et al. 2003, and the EROS alert system<sup>3</sup>), and OGLE (Jaroszyński 2002). We found two more binaries in addition to the ones that failed the  $\chi_{\text{ml}}^2$  condition: SC21-45456 (97-BLG-1; Alcock et al. 2000a), in which only the declining part of the light curve is covered by the OGLE data, and SC20-69068 (sc20-1793; Jaroszyński 2002), where the observed deviations are small. All four binary lens candidates and their corresponding ID cross-references are listed in Table 3. A complete list of cross-references for our candidate events is available electronically on ApJ-web.

In case of binary lens events it is difficult to find reliable lensing parameters like  $t_E$  and  $I_s$  without very good coverage. Unfortunately, that is the case for most of our candidates. Furthermore, it is a complicated task to estimate the detection efficiency for binary microlensing. The fraction of binary lens events is around 3–8% (Alcock et al. 2000a; Jaroszyński 2002; Jaroszyński et al. 2004). In §5 this fraction is used to account for the optical depth contribution from binary lens events. This avoids estimating  $\tau$  due to individual binary lenses, which is subject to large uncertainties in our sample.

One of the events, namely SC33-553617 (sc33\_4505 in Smith, Mao & Woźniak 2002), is a strong parallax event, and is included in the optical depth measurement in §5. None of the remaining candidate parallax events listed in Smith, Mao & Woźniak (2002) are part of our sample, including possible parallax events with weak signatures.

### 3.5. Rejecting events with faint, strongly blended sources

In this section we look for evidence of blending using only information from light curve fitting. Model degeneracy is known to be a severe problem (Woźniak & Paczyński 1997; Han 1999; Bond et al. 2001; Gould & An 2002). It was therefore of critical importance, that all 62 events in our level 5 sample have exceptionally high S/N ratio and very good coverage. This allowed us to make use of the fitted lensed flux fraction  $f_S = F_s/(F_s + F_b)$  and its error. Fig. 3 shows the resulting relation between the apparent magnitude of the total light ( $I_{\text{total},0}$ ) and the best fit source magnitude ( $I_{s,0}$ ), both corrected for extinction. Considering a positive error range  $\sigma_{I_{s+}}$  we can construct an upper limit for the source magnitude as  $I_{s,0} + \sigma_{I_{s+}}$ . This leads to an unexpected conclusion that, with high probability, in 29 out of 62 events the source may actually be below  $I_{\text{RC,th}}$  and does not satisfy level 0 conditions. In other words, the actual source in such an event merged with a much brighter star to make a single PSF peak detected by the DoPHOT code. For such events the detection

---

<sup>3</sup>[http://dphs10.saclay.cea.fr/Spp/Experiences/EROS/alertes.html](http://dphs10.saclay cea.fr/Spp/Experiences/EROS/alertes.html)



efficiency cannot be estimated assuming one possible lensed star per database light curve. We remove those 29 events (level 6, Table 2) and for the optical depth estimate we use only the remaining 33 high quality events with low probability of having  $I_{s,0} > I_{RC,th}$ . There are 32 unique events because SC31-111306 and SC30-717699 are the same event found in the overlap region between two fields. Here we limit the discussion to light curves and selecting the final event sample. Our unexpected result prompted a much more rigorous analysis of blending and a detailed discussion is deferred to § 6.2.

We note a relatively large number of events detected in field BUL\_SC30 compared to the neighboring fields SC22 and SC23. Popowski et al. (2004) detected a similar excess at a location about 1 deg away. It remains to be established whether these fluctuations imply a statistically significant clustering of microlensing events.

Light curves of 33 microlensing events in the final optical depth sample are shown in Fig. 4, and their best fit parameters are listed in Table 4. In case of SC33-553617 we also fitted a parallax model, in addition to a standard single lens model. The best fit parallax model is shown as dotted line in Fig. 4 and its parameters are given in Table 4. Using the notation from Soszyński et al. (2001) we found  $\psi = 3.17 \pm 0.12$  rad and  $\tilde{r}_E = 6.16 \pm 0.39$  AU for the heliocentric orientation of the lens trajectory and the Einstein ring radius at the observer plane, respectively. These values differ by about  $2.7 \sigma$  from results in Smith, Mao & Woźniak (2002). The discrepancy is insignificant and fully accounted for by slight differences in the selection of good science frames and the details of photometric calibrations.

In Table 5 we list level 5 events that were rejected for blending at level 6. Examples of light curves from the group showing evidence for blending are plotted in Fig. 5. For better readability Tables 4 and 5 only contain symmetric (parabolic) 68% confidence level intervals. The analysis uses proper asymmetric confidence intervals for 1 parameter of interest. Complete information on model fits and their uncertainties is available in the electronic form from ApJ web. Supplemental files include a complete list of cross-references of our microlensing events with other published work, as well as other parameters and event samples that could not fit comfortably in this paper.

#### 4. Detection efficiency

We estimate this crucial ingredient of the microlensing optical depth measurement in a two-step process. In the first part we construct a synthetic reference image for each field to simulate blending of stellar flux and the effects of source confusion on object catalogs in OGLE-II (see § 6.2 for a detailed discussion of blending). The second part deals with the

ability to detect microlensing events in database light curves known as sampling efficiency. This reflects the way our actual data set was processed. Stars were detected and their positions were measured on reference images using the DoPHOT code. In order to reduce photometric noise the DIA software was later used to measure fluxes. The transformation of the difference flux to standard magnitudes also involves DoPHOT photometry, which determines the baseline flux.

#### 4.1. Blending distributions from synthetic images

Synthetic stars were drawn from a luminosity function (LF) derived separately for each field. We made composite LFs with the bright end based on the photometric maps of Udalski et al. (2002). The faint end of the LF, in all fields, was taken to be the same as the HST LF in the Baade’s Window (Holtzman 1998), except for adjustments due to variable field extinction and Galactic bar geometry (compare Sumi 2004). Both pieces have good completeness near  $I_0 = 16$  mag, where they were joined and normalized. We constructed synthetic reference images starting from a flat Poisson background. Those images were further populated with stars at random positions down to the extinction free magnitude  $I_0 \sim 21.0$  mag, matching the observed number density of bright stars in the field. The PSF flux of each star was reduced according to the extinction map in Sumi (2004) interpolated at the appropriate position from a  $\sim 30''$  resolution. Local PSF shapes were also determined on a star by star basis using spatial PSF models from Woźniak (2000). Poisson noise was added in the amount that approximated the statistics of real reference frames. Those simulated frames were processed with DoPHOT and the output source catalog was constructed using procedures identical to those in the preparation of the real database. For each simulated star in the input list we found the closest star in the output DoPHOT catalog. Obviously, the number of detected stars is much lower than the number of simulated stars due to blending, but also because at some low flux level the GB stars are so numerous that they form a smooth background.

In Fig. 6 we show the relation between the extinction corrected  $I$  magnitude of the input star ( $I_{\text{in},0}$ ) and the closest output star ( $I_{\text{out},0}$ ). One can see that a large majority of bright stars is recovered correctly, however great numbers of faint simulated stars “come out” as random bright stars. A faint star has a very high probability of blending with a bright star to form an even brighter catalog source. This is best studied by Monte-Carlo simulations because the ability to separate close stars in the photometric code depends in a complicated way at least on the flux, the flux ratio, the separation and the PSF shape. Each star from the input LF has equal probability of microlensing, so Fig. 6 can be transformed into a relation

between the blending parameter  $f_S$  and  $I_{\text{out},0}$  as shown in Fig. 7. This is simply a prior probability that the lensed flux is a fraction  $f_S$  of the total flux, given a random event with the observed magnitude of the composite  $I_{\text{out},0}$ . Histograms of  $f_S$  were obtained by binning the map in Fig. 7 into 0.2 mag intervals of  $I_{\text{out},0}$ , and were used in the next step to generate random events in the efficiency simulation on database light curves. Fig. 8 presents some examples.

It must be stressed that our blending distributions are subject to some (small) uncertainties intrinsic to the simulation. IDs of merging objects need to be traced between the simulated input and output catalogs, which does not take place during the construction of the photometric database (§2). The exact allocation of flux to detected objects is affected by the finite accuracy of positions and the photon noise interacting with the deblending code.

#### 4.2. Light curve sampling efficiency

In order to simulate real sampling and photometric accuracy we “inject” additional flux and photon noise into actual light curves, randomly selected from the group searched for microlensing (§3). Simulated events have random input parameters drawn from flat distributions:  $0 < u_{\text{min}} < 1$ ,  $2450530 < t_0 < 2451860$  JD and  $\log(1 \text{ d}) < \log(t_E) < \log(500 \text{ d})$ . The blending parameter  $f_S$  is drawn from one of the histograms made in the previous section according to the baseline magnitude (Fig. 8). The shape of this histogram varies depending on how deep we integrate in  $I_{\text{in},0}$ . The efficiency for faint stars is low and very time consuming to compute, so we looked at possible improvements. A preliminary simulation was conducted for BUL\_SC3 (one of the densest OGLE-II fields) by generating 20,000 events down to  $I_{\text{in},0} < 20$ . We strictly repeated the event selection process from §3. Figs. 9 and 10 compare the most important simulation results to observed distributions. In §6.2 we will use this information to better understand blending effects.

From the data shown in the top-right panel of Fig. 10 we find that only 1% of events in the simulated optical depth sample have input source stars fainter than our brightness threshold  $I_{\text{RC,th}}$ . We verified that this fraction remains very low for other distributions of  $t_E$ . Then we can safely assume  $I_{\text{in},0} < I_{\text{RC,th}}$  when constructing the histograms of  $f_S$  for subsequent simulations, i.e. we use stars below the dashed line in Fig. 7. It means that our simulated source LF is the one actually measured by the OGLE-II experiment, making our calculations very insensitive to uncertainties in the faint part of the LF. (Sufficiently deep HST data are currently available only for Baade’s window.) The actual detection efficiency in each field is computed from 20,000 simulated events with blending down to  $I_{\text{RC,th}}$  and integrated over all parameters except  $t_E$ . The results for BUL\_SC3 field are plotted in

Fig. 11. They are very similar for other fields, which are available electronically on ApJ-web. These efficiencies are reduced by about 10% when compared to the case without blending, because the main peak in  $f_S$  is near 0.9 for most stars in our RCG region.

## 5. Microlensing optical depth

The optical depth  $\tau$  can be defined as the probability that a random star is microlensed with the impact parameter  $u_{\min} \leq 1$  at any given time. It can be estimated as

$$\tau = \frac{\pi}{2N_s T_o} \sum_i \frac{t_{E,i}}{\varepsilon(t_{E,i})}, \quad (6)$$

where  $N_s$  is the total number of source stars monitored for microlensing,  $T_o$  is the duration of the survey in days,  $t_{E,i}$  is the event time-scale for the  $i$ -th event, and  $\varepsilon(t_{E,i})$  is the detection efficiency at that time-scale. In our case  $N_s = 1,084,267$  and  $T_o = 1330$  d.

Blending simulations in §4.1 show that stars below our magnitude threshold have practically no chance to contribute detectable events. This allows us to simplify and speed up the calculation by only simulating stars with  $I_{s,0} < I_{RC,th}$ , but also has a side effect of giving about average efficiency to a small percentage of simulated stars which crossed the threshold and have practically no efficiency in the actual survey. Equivalently, with the efficiency computation from §4.2, the number of sources that can be lensed is slightly overestimated due to blending. In principle, the effect can be corrected by lowering  $N_s$  in Equation 6 according to the ratio between the input and output LFs integrated above  $I_{RC,th}$ . Depending on the field, the resulting optical depth would increase by 7–12 %, or  $\sim 9\%$  on average. The size of the correction is uncertain by a factor  $\sim 1.5$  due to several competing biases at a few percent level. To name a few, they include: limited accuracy and source confusion intrinsic to our image simulations (§4.1), occasional DoPHOT artifacts in the database, and second order effects like not counting in  $N_s$  a tiny fraction of “balanced” blends above the magnitude threshold (those with  $f_S \sim 0.5$  and near the bright end of the LF; see §6.2.2). Over-counting of RCG sources is partially canceled by about 2% due to artificial events having  $I_{s,0} > I_{RC,th}$ , an effect caused by using 0.2 mag bins to store the  $f_S$  distribution (see Fig. 8). Those stars cannot produce detectable events in our simulation. In the end, we rescaled the optical depth and the error by  $9 - 2 = 7\%$ .

According to the level 5 criteria (Table 2), all four binary lens events were removed from the optical depth sample. The model parameters of those events (including  $t_E$ ) are poorly constrained, and their RCG membership is uncertain. The fraction of binary lens events

among all microlensing events has been estimated at 8% (Jaroszyński 2002), 6% (Alcock et al. 2000a), and 3% (Jaroszyński et al. 2004). In our RCG sample, we found evidence for a binary lens fraction  $4/62 = 0.06$ , in good agreement with previous work. We use this value to correct our optical depth measurement for binary lens events excluded from the sample. Assuming that the lens system consists of two stars having the same typical time scale, the optical depth contribution of a binary lens event is  $2^{1/2}$  times that of a single lens event. The ratio between the number of events with binary lenses and single lenses is  $0.06/(1 - 0.06)$ . It follows that the optical depth values and their errors have to be rescaled by a factor 1.09.

Individual optical depth estimates for each field are listed in Table 1. The errors were estimated using the formula of Han & Gould (1995). We also estimated the average optical depth in all 20 fields combined, and found  $\tau = 2.55_{-0.46}^{+0.57} \times 10^{-6}$  at  $(l, b) = (1.^{\circ}16, -2.^{\circ}75)$ . The effective line of sight was computed by weighting field centers with the number of source stars in each field. Here the error was estimated using a Monte-Carlo method from Alcock et al. (1997), which is consistent with a value  $\pm 0.47$  from the formula of Han & Gould (1995).

The left panels of Fig. 12 show the microlensing optical depth from OGLE-II bulge data as a function of the Galactic coordinates  $b$  and  $l$  (filled circles). Fields were binned in ranges  $\Delta b, \Delta l = 0.5^{\circ}$  with  $l$  and  $b$  averaged in each bin. The errors are estimated according to Han & Gould (1995). Although there is no correlation in  $l$ , we can see a trend in the optical depth along  $b$ . A simple linear fit gives  $\tau = [(4.48 \pm 2.37) + (0.78 \pm 0.84) \times b] \times 10^{-6}$ . In Fig. 12 we also compare the average  $\tau$  from this work (open circle) with values published by Popowski et al. (2004) (open diamond) and by Afonso et al. (2003) (open square). All three measurements are roughly consistent. They fall well below the results in Alcock et al. (2000b) and Sumi et al. (2003) based on all survey stars regardless of brightness ( $\tau \sim 3.3 \times 10^{-6}$  at  $b \sim -3.^{\circ}5$ ). However, the latter values include a dubious upward correction by about 20% for the presence of disk stars that rarely produce events, and the uncorrected estimates ( $\tau = 2.43_{-0.38}^{+0.39} \times 10^{-6}$  and  $2.59_{-0.64}^{+0.84} \times 10^{-6}$ , respectively) are only  $\sim 1.5\sigma$  higher than our present result. When comparing estimates made by various experiments, we adjust for the measured gradient of  $\tau$ . Our new optical depth value is also consistent with predictions based on the revised COBE bar model by Han & Gould (1995), which has the mass  $M_{\text{bulge}} = 1.62 \times 10^{10} M_{\odot}$  and the viewing angle  $\phi \sim 20^{\circ}$ , and the latest COBE elongated bar model by Bissantz & Gerhard (2002) with  $\phi \sim 20^{\circ}$ .

For comparisons, the right panels of Fig. 12 show the effect of removing the parallax event. The lens that caused the parallax event is most likely in the disk. The sample without the parallax event is more representative of the bulge structure and less influenced by the disk component, giving  $\tau = [(4.86 \pm 1.94) + (1.01 \pm 0.65) \times b] \times 10^{-6}$ . The gradient of  $\tau$  along  $b$  becomes more clearly visible in this case, as one would predict based on the GB models.

In §6.2.3 we use a control sample to further investigate the systematics associated with various methods of estimating  $\tau$  and discuss a possible difference between results based on samples selected using models with and without blending.

## 6. Discussion

### 6.1. Results from microlensing model fits

Here we discuss distributions of the best fit microlensing parameters for our events. In this section event SC31-111306 is not included because it is identical with SC30-717699.

#### 6.1.1. Blending parameter

The histograms of  $f_S$  are shown in Fig. 9 (top-left). The solid line is for 32 events in the final optical depth sample, while the dotted line represents all 61 events at level 5. The remaining panels in this figure show the relevant results from Monte-Carlo simulations in §4. As intended, our level 6 condition removed events which appeared to be highly blended photometrically. In the remaining events  $f_S$  is symmetrically distributed around the peak at  $f_S = 1$ .

There are several events with “negative blending”, i.e.  $f_S > 1$ . It is not allowed theoretically, but also not uncommon in fits to real data. Such unphysical best fit parameters arise due to several factors including: near degeneracy of the model in the presence of statistical fluctuations, systematic errors in photometry (e.g. from a centroid bias or an imperfect deblending), occasional “holes” in the background of unresolved faint stars (Park et al. 2004), or assuming an incorrect model. In our data set the first two effects explain most cases. We allow formally  $f_S > 1$  to avoid a systematic bias in the microlensing parameters.

In Fig. 10 (top-left) we show histograms of  $I_{s,0}$ , the extinction corrected source magnitude. Again, the solid line represents 32 events in the optical depth sample, while the dotted line is for all 61 events in the level 5 sample. The remaining panels in this figure are for comparisons with Monte-Carlo simulations. The dashed vertical line indicates the magnitude threshold  $I_{RC,th}$  adopted for BUL\_SC3 field. The original goal of the blending analysis was to place a reasonable upper limit on the number of blends and derive  $\tau$  assuming  $f_S = 1$  in RCG events, perhaps after applying a small blending correction to the ingredients going into the estimator. Instead, for about half of apparently bright OGLE-II events we found  $f_S$  and  $\sigma_{f_S+}$  that likely puts the actual source well below the magnitude threshold  $I_{RC,th}$ . In

§6.2.1 this surprising observation is reconciled with simulations.

### 6.1.2. Impact parameter and time-scale

In Fig. 13 we show a cumulative histogram of the best fit impact parameter for our 32 events. It shows a slight discrepancy with respect to a uniform distribution in  $u_{\min}$ . The KS test gives a 3.4% probability for this departure from uniformity to occur by chance, not alarming in case of this particular type of test. Popowski et al. (2004) find a very similar feature. Slightly low detection efficiencies at large  $u_{\min}$  and significant noise in the best fit parameters while  $u_{\min}$  is forced to be positive will tend to produce the observed pattern.

The corresponding histogram of  $t_E$  is shown in Fig. 14 (top). The mean time-scale is  $\langle t_E \rangle = 32.8 \pm 4.8$  d without any correction for detection efficiency. This is close to the value of 30 d obtained by Popowski et al. (2004). A proper comparison with other results and theoretical estimates requires weighting the histogram in Fig. 14 by the inverse efficiency (bottom). The corrected mean time-scale is  $\langle t_E \rangle = 28.1 \pm 4.3$  d, while Popowski et al. (2004) found  $\langle t_E \rangle = 15$  d. Wood & Mao (2005) have recently compared several measured time-scale distributions to predictions from a Galactic model adopted from Han & Gould (2003), after it was empirically normalized by star counts. Wood & Mao (2005) found that our corrected  $t_E$  distribution (preprint) is in good agreement with their model, while the results in Popowski et al. (2004) show an excess of short-duration events. The discrepancy is likely to originate from a different treatment of blending (§6.2.3). Our corrected value is longer than the prediction from the model by Bissantz, Debattista & Gerhard (2004). It is also below 45 d predicted by a bar model rotating at  $v_{\text{rot}} = 50$  km/s, but significantly longer than 14 d without any streaming motion estimated by Evans & Belokurov (2002). Therefore, the OGLE-II data provide some support for the existence of streaming motions in the Galactic bar. Further analysis of the bar kinematics is beyond the scope of this paper.

## 6.2. How important is blending in bright stars ?

### 6.2.1. Photometric evidence for strong blends

As mentioned in §6.1.1 the data of the kind shown in Fig. 3 suggest that in many OGLE-II events the true source is much fainter than it appears. It is somewhat unexpected that a fraction of such events should reach  $\sim 50\%$ , a value suggested by the number of events rejected at level 6. On closer look, however, a brief inspection of model fits for hundreds of the OGLE-III events from the Early Warning System (EWS; Udalski 2003) supports this

finding. As many as 20% of sources brighter than 16 mag are still severely blended in more densely sampled and better resolved OGLE-III images. The results from image simulations (§ 4.1) help to clarify the issue.

In the top-left panel of Fig. 9 the observed distribution of the blending parameter  $f_S$  for level 5 events (dotted line) peaks at a low value below 0.1. Despite a large spread in  $f_S$  introduced by model fitting, this is inconsistent with  $f_S = 1$  in all level 5 events according to the simulation results depicted in the bottom-left panel of Fig. 9. The opposite is true for level 6 events. The observed sample is fully consistent with “no blending” scenario (solid lines).

We also verified how efficient are level 6 criteria in rejecting most blending without removing too many unblended events. Note that our conservative magnitude threshold employs the formal error  $\sigma_{I_{s+}}$  in addition to the intrinsic source magnitude  $I_s$  (both from model fits). From Fig. 10 we find that out of all simulated events which make it to the optical depth sample, only 1% has  $I_{s,0} > I_{RC,th}$  (top-right). At the same time only about 16% of unblended events are lost that way (bottom-left). The near degeneracy of the model is broken more often with high S/N light curves delivered by DIA photometry. Some loss of efficiency was still unavoidable in cases of strong degeneracy, because we insisted on keeping the contamination from faint blends at a low level. Finally, the fraction of simulated events rejected for blending is very close to that in the sample of actual observed events, i.e.  $\sim 50\%$  (Figs. 9 and 10), further strengthening the evidence for numerous blends.

The fraction of blended events relative to all events can be estimated using the statistics collected from the simulation. The number of events which passed level 5 and 6 is  $N_5 = 2886$  and  $N_6 = 1502$ , respectively (bottom-right panel of Fig. 10). Taking into account the fact that 16% of RCG events fail the level 6 cut, the number of real RCG events at level 5 is given by  $N_{cand,RCG} = 1502/(1 - 0.16) = 1788$ . Then the number of blended events is given by  $N_{cand,blend} = N_5 - N_{cand,RCG} = 1098$ , which is 38% of  $N_5$ . Using the observed events we have  $N_{cand,RCG} = 38$  and  $N_{cand,blend} = 23$ , so an estimated 38% of all events are blended events. This is fully consistent with our simulation.

Afonso et al. (2003) studied blending in the EROS bulge survey data. Using a pixel level simulation they found that in the EROS bright star sample the fraction of events due to blends is  $\sim 38\%$ . However, the EROS analysis was based on a microlensing model without blending, unless it produced unacceptable  $\chi^2$ . In § 6.2.3 we show that this would imply even more blended events in hypothetical EROS samples selected using a model that allows for blending. Nevertheless, both OGLE and EROS image simulations indicate that blends are fairly common in RCG samples.



### 6.2.2. Astrometric evidence for strong blends

Some strong blends betray their presence by showing a detectable centroid shift of the combined light. While in principle this information can be used to reject blended events, applying astrometric selection criteria is complicated in practice. Another problem is that positions of some blends are aligned within the measurement errors. Sensitivity can be improved by comparing an unbiased position from stacked difference frames with the mean centroid of the composite. Even then, the maximum observable shift is  $(1 - f_s)$  times the separation of the blend (for a baseline dominated reference frame).

Despite these limitations we looked for astrometric shifts to check for consistency with the photometric evidence. In Fig. 15 we plot the differences between source positions in the reference image, typically dominated by the baseline, and a stack of difference images taken near the peak magnification. Out of 32 level 6 events (left) only two show a clearly detected shift above 0.2 pixels ( $\sim 0.08''$ ). That fraction increases dramatically to 28% for level 5 events (left and right combined) and is entirely consistent with the value  $\sim 30\%$  predicted from a distribution of blend separations in our simulated images with the detection efficiency as a function of  $f_s$ . As expected, the largest shifts in Fig. 15 are observed for strong blends with low  $f_s$ . Therefore, we have an independent confirmation that, for bright stars, the DIA photometry alone is sufficiently effective in rejecting strong blends in OGLE-II data. Please note that the relevant selection criteria in Table 2 admit blended events as long as the best fit source magnitude is  $1\sigma$  above the threshold. This occurs only for a tiny fraction of bright stars (Fig. 8) and has negligible influence on the optical depth.

### 6.2.3. Blending, parameter bias and derived optical depths

In previous sections we showed that samples of microlensing events with apparently bright sources still contain many strong blends. This holds for any survey with seeing comparable to or worse than the median FWHM  $\sim 1.3''$  in OGLE-II, assuming a similar density of stars. It may then seem counterintuitive, that our measured optical depth (adjusted for the gradient) agrees with the values recently found by Afonso et al. (2003) and Popowski et al. (2004), who used microlensing parameters based on a model without blending to select their RC samples. To investigate this issue we reintroduced the latter method into our analysis of the OGLE-II extended RC sample. We performed microlensing model fits with the blend flux fixed at  $F_b = 0$ , followed by a selection of events using the same criteria as before (Table 2). Note that the requirement on the source magnitude at level 6 is now identical to the second condition at level 0. This procedure selected 48 good quality events, all of which were confirmed visually. This control sample was not screened for blending and is 1.5 times

larger than the one used to calculate the optical depth (§5). Its sole purpose is to compare our analysis with previous work (Afonso et al. 2003; Popowski et al. 2004), particularly to assess the level of bias in the best fit parameters and the impact on the derived optical depth.

In Figs. 16 and 17 we compare the results of the model fitting with and without blending. From §3 we show the sample of 32 level 6 events (filled circles) and its level 5 superset (open circles). We also plot the control sample of 48 events introduced for comparisons (open squares). There are 30 events common between all three samples. The control sample includes 10 events rejected as blends in the optical depth analysis. In events showing no evidence for blending there is little difference between the best fit model with fixed  $f_S = 1$ , and the one with freely variable  $f_S$ . For the remaining (blended) events we confirm that forcing  $F_b = 0$  gives overestimated  $u_{\min}$  and underestimated  $t_E$ , a well known fact. There are 3 events in which  $t_E$  significantly increases after fixing  $f_S = 1$ . Those have “negative blends”, i.e.  $f_S > 1$  (§6.1.1). Before the efficiency correction, the control sample had the mean  $t_E$  of 35.8 and 25.5 d corresponding to the model fits with and without blending. Event SC37-485133 has the best fit  $t_E = (3.4 \pm 3.4) \times 10^4$  d when  $f_S$  is allowed to be optimized and was removed from the estimates of the mean time-scale.

The detection efficiency  $\varepsilon(t_E)$  in the control sample was computed following the methods in §4 except that simulated events were assumed to have  $f_S \equiv 1$ , as in Afonso et al. (2003) and Popowski et al. (2004). The result for BUL\_SC3 field is shown in Fig. 18. Assuming no blending, the efficiency is 30% higher on average compared to  $\varepsilon(t_E)$  in a blended scenario (Fig. 11), largely because fixing the blending parameter amounts to less degeneracy.

The optical depth estimate with the control sample is consequently  $\tau = (1.97 \pm 0.35) \times 10^{-6}$ , where the error is from Han & Gould (1995) formula. Although  $1\sigma$  lower than our main result, this value explicitly demonstrates a near cancellation of the two major competing biases discussed by Afonso et al. (2003) and Popowski et al. (2004). The efficiency corrected mean time-scale in the control sample is  $\langle t_E \rangle = 21.9 \pm 3.2$  d, shorter by 20% than  $\langle t_E \rangle = 28.1 \pm 4.3$  d estimated in §6.1.2. Event selection using model fits with  $f_S \equiv 1$  produced a sample of roughly 50% more events with  $t_E$  underestimated by  $\sim 20\%$  and  $\varepsilon(t_E)$  higher by  $\sim 30\%$ . Although the latter assumption is incorrect, it leads to a final value of the optical depth that is statistically indistinguishable from the one we found using a proper model. Note that an estimated 2/5 out of 50% more events stated above are real RCG events, knowing that 16% of real RCG events fail the level 6 cut (see §6.2.1). So, the fraction of blended events in the control sample is  $\sim 20\%$  (30/150), consistent with 19% from Fig. 16 and similar to 17% estimated by Popowski et al. (2004) in MACHO RCG sample.

The difference between optical depth estimates based on two different treatments of blending in our data is at an inconclusive  $1\sigma$  level. Generally, it is possible that one of these methods of estimating  $\tau$  is more biased than the other. Such bias might have contributed to somewhat higher  $\tau$  values from analyses based on blended microlensing fits (Alcock et al. 2000b; Sumi et al. 2003 and § 5 in this paper), compared to values based on fits without blending (Popowski et al. 2004; Afonso et al. 2003 and our control sample). The issue warrants further investigation, however finding a reliable answer will likely require very detailed simulations that are beyond the scope of this paper.

It should be emphasized how risky is the argument that unblended fit can be used when introducing it into the model does not significantly lower the  $\chi^2$ . The more blending in the event, the more degenerate is the model fit. With a typical S/N stronger blends are actually harder to find using  $\chi^2$  improvements. We have evidence for heavy degeneracy in 12 of our level 4 candidates, and mild degeneracy in many more cases. Despite having little effect on the optical depth estimate, neglecting blends biases time-scale distributions and event rates. The degree of cancellation likely depends on the specifics of each dataset, e.g. typical seeing, and eventually will no longer be “perfect” as statistical errors continue to shrink.

#### 6.2.4. *Effects of weak parallax and binary events on optical depth*

In low S/N events, a 5-parameter model fit with blending is substantially more degenerate than a corresponding 4-parameter fit with  $f_s \equiv 1$ , and can be sensitive to small changes in the data. Such low level light curve deviations may be caused by weak exotic events, most commonly by parallax and binary lens events. The problem with this type of deviations is that they are hard to include in simulated events, so they are typically ignored in the detection efficiency calculations. It is an open question whether the presence of those weakly exotic events in samples selected using a 5-parameter model introduces a bias in the optical depth. The issue has not been sufficiently studied. A correction for such hypothetical bias could in principle be obtained from extensive simulations that account for the Galactic Disk geometry, but such calculations are not available today.

There is some evidence that weakly exotic events are not significantly biasing our measurement. A thorough search for parallax events (including weak signals) has been performed by Smith, Mao & Woźniak (2002) using the first 3 years of the OGLE-II data. Out of 512 candidate microlensing events, a single convincing event (herein SC33-553617) and 5 more marginal parallax events were found (after excluding two events that are actually binaries). The fraction is about 1 %. Parallax events are most likely due to disk lenses whose fraction is rather uncertain and estimated at 10–20 % from disk models. Moreover, the expected

time-scale is 50 days or more, so only 10–20 % of all events are relevant here. Therefore, we expect that only a few per cent of the events have parallax effects. Knowing that 1 event has already been found in the sample, we expect negligible contribution from parallax events beyond what is already included.

In case of binary events, the binary fraction from published work is 3–8 %, and we correct the measurement using our own estimated 6 % fraction. We do not expect more significant binary lens events. Any bias in the optical depth due to a combination of subtle light curve changes and fitting 5-parameter models would have to be accounted for. However, to our best knowledge, such bias has not been reported.

## 7. Summary and conclusions

We found 81 microlensing events in a sample of about 1 million bright source stars in the extended RCG region. Light curves for 62 of those events are well represented by a single lens model with relatively small uncertainty in the best fit parameters. In the latter sample we investigated blending and concluded that about 38% of microlensing events with the apparent RCG sources are actually due to fainter stars below the magnitude threshold. This large value for the fraction of blended events is fully supported by our extensive Monte-Carlo simulations of source confusion in the OGLE-II reference images.

The microlensing optical depth was estimated using 32 high S/N events whose source stars are still in the extended RCG region. We measured  $\tau = 2.55_{-0.46}^{+0.57} \times 10^{-6}$  at  $(l, b) = (1.^\circ 16, -2.^\circ 75)$ . Considering our estimate of the gradient along the Galactic latitude  $b$ ,  $\tau = [(4.48 \pm 2.37) + (0.78 \pm 0.84) \times b] \times 10^{-6}$ , this value is consistent with recent measurements based on RCG source stars by Popowski et al. (2004) and Afonso et al. (2003).

Our goal was to ensure a high quality measurement of  $\tau$  using RCG stars in the Galactic Bulge. The result presented here is based on a rigorous treatment of source confusion and a relatively large number of well sampled high S/N events, with the purpose of minimizing uncertainties in  $t_E$  and in the number of events. It may therefore seem surprising that our result is not out of line with the values obtained by Popowski et al. (2004) and Afonso et al. (2003), who selected RCG samples using an unblended model. On the other hand, these authors have also argued that the two dominant biases nearly cancel each other. The contribution due to an underestimated number of monitored sources has the opposite sign to that from underestimated time-scales in blending free model fits. We tested the hypothesis of near cancellation of the bias by reanalyzing our microlensing sample. Indeed, under the no blending assumption we found nearly the same value of  $\tau = (1.97 \pm 0.35) \times 10^{-6}$  with

roughly 50% more events, 20% lower  $t_E$  and 30% higher detection efficiency. This does not change the fact that such procedure shifts the distribution of time-scales to lower values by significant amount and makes it hard to study the kinematics of the source/lens populations.

The efficiency weighted mean time-scale in our sample of 32 events is  $\langle t_E \rangle = 28.1 \pm 4.3$  d, which is significantly longer than 15 d estimated by Popowski et al. (2004). This is not as long as 45 d predicted by models with the streaming motion of the bar, but significantly longer than 14 d without any streaming (Evans & Belokurov 2002). Therefore, our result implies some streaming in the bar (first measured by Sumi, Eyer & Woźniak 2003). Further analysis of the time-scale distribution is planned including the information in the OGLE-II proper motion catalog (Sumi et al. 2004a).

Our value of  $\tau$  agrees with predictions from Han & Gould (1995) model with the bulge mass  $M_{\text{bulge}} = 1.62 \times 10^{10} M_\odot$  and the viewing angle  $\phi \sim 20^\circ$ . It is also consistent with microlensing optical depths derived by Evans & Belokurov (2002) using Galactic bulge models of Dwek et al. (1995) and Binney, Gerhard & Spergel (1997).

It has been noted that  $\tau$  measurements based on RCG stars (Afonso et al. 2003; Popowski et al. 2004) fall systematically below the estimates using all sources down to the detection limit, including recent DIA results (Alcock et al. 2000b; Sumi et al. 2003). The difference persists, although at a lower level, when the dubious correction for disk stars is not applied. We are not aware of a convincing detailed explanation of this gap, although source confusion and model degeneracy biasing  $t_E$  and  $u_{\text{min}}$  are prime suspects. Alternatively, the difference may be related to the treatment of blending. The significance of any potential biases due to near degeneracy of the 5-parameter microlensing curve should be established. The systematics of event selection using model fits with free  $f_S$  (Alcock et al. 2000b; Sumi et al. 2003, and this work) and with  $f_S \equiv 1$  (Afonso et al. 2003; Popowski et al. 2004) may be the culprit. Another area of concern for wider use of the blended microlensing curve is a possible perturbing effect on the optical depth due to the presence of unrecognized weakly exotic events discussed in §6.2.3 and §6.2.4.

The event selection criteria in this analysis strongly discriminate against a high level of degeneracy in the fit (§3.3). It is our goal to estimate  $\tau$  using all events of any magnitude and investigate the source of the above discrepancy. A good understanding of the involved statistics will allow tapping into a much larger set of useful events. As of 2005, in the GB fields the OGLE-III survey detects about 600 events per year. According to Han & Gould (1995) one needs roughly 700–800 events to distinguish a barred Galactic bulge from its axisymmetric alternative, and with  $\sim 1800$  events we can hope for a  $3\sigma$  measurement of the relative contributions from the bulge and disk components. Future statistical modeling of the microlensing survey data needs to reflect source confusion effects, still evident among

bright stars.

We acknowledge A. Gould, O. Gerhard and M. Smith for helpful comments. TS acknowledges the financial support from the JSPS. PW was supported by the Oppenheimer Fellowship at LANL. This work was partly supported with the following grants to BP: NSF grant AST-0204908, and NASA grant NAG5-12212. The OGLE project is partly supported by the Polish KBN grant 2P03D02124 to AU.

## REFERENCES

- Afonso, C. et al. 2003, *A&A*, 404, 145
- Alard C., 2000, *A&AS*, 144, 363
- Alard C., Lupton R. H., 1998, *ApJ*, 503, 325
- Alcock, C. et al. 1997, *ApJ*, 486, 697
- Alcock C. et al., 2000a, *ApJ*, 541, 270
- Alcock C. et al., 2000b, *ApJ*, 541, 734
- Binney, J. et al. 2000, *ApJ*, 537, L99
- Binney, J. Gerhard, O. & Spergel, D. 1997, *MNRAS*, 288, 365
- Bissantz, N. & Gerhard, O. 2002, *MNRAS*, 330, 591
- Bissantz, N., Debattista, V. P. & Gerhard, O. 2004, *ApJ*, 601, L155
- Bond I. A. et al., 2001, *MNRAS*, 327, 868
- CERN Lib., 1998, <http://wwwasdoc.web.cern.ch/wwwasdoc/minuit/minmain.html>
- Evans N.W., & Belokurov, 2002, *ApJ*, 567, 119
- Dwek, E. et al. 1995, *ApJ*, 445, 716
- Gould, A. & An, J. H. 2002, *ApJ*, 565, 1381
- Griest, K., et al. 1991, *ApJ*, 372, L79
- Gyuk, G. 1999, *ApJ*, 510, 205

- Han, C. & Gould, A. 1995, *ApJ*, 449, 521
- Han, C. 1999, *MNRAS*, 309, 373
- Han, C. & Gould, A. 2003, *ApJ*, 592, 172
- Holtzman, J. A. 1998, *ApJ*, 115, 1946
- Jaroszyński, M., 2002, *Acta Astronomica*, 52, 39
- Jaroszyński, M. et al., 2004, preprint, astro-ph/0408243
- Kiraga, M., & Paczyński, B. 1994, *ApJ*, 430, L101
- Paczynski, B. 1986, *ApJ*, 304, 1
- Paczynski, B. 1991, *ApJ*, 371, L63
- Paczynski, B. et al. 1994, *ApJ*, 435, L113
- Paczynski, B. 1996, *ARA&A*, 34, 419
- Palanque-Delabrouille, N., et al. 1998, *A&A*, 332, 1
- Park, B. -G. et al. 2004, *ApJ*, 609, 166
- Peale, S. J. 1998, *ApJ*, 509, 177
- Popowski, P. et al. 2001, in *ASP Conference Series: Microlensing 2000: A New Era of Microlensing Astrophysics*, eds. J.W. Menzies & P.D. Sackett (San Francisco: Astronomical Society of the Pacific), Vol. 239, p. 244, (astro-ph/0005466)
- Popowski, P. et al. 2004, preprint (astro-ph/0410319)
- Schechter, L., Mateo, M., & Saha, A., 1993, *PASP*, 105, 1342S
- Smith M. C., Mao, S. & Woźniak, P. R., 2002, *MNRAS*, 332, 962
- Soszyński, I. et al. 2001, *ApJ*, 552, 731
- Sumi, T., 2004, *MNRAS*, 349, 193
- Sumi T., Eyer, L. & Woźniak, P. R., 2003, *MNRAS*, 340, 1346
- Sumi, T. et al., 2003, *ApJ*, 591, 204
- Sumi, T. et al., 2004a, *MNRAS*, 348, 1439

- Sumi, T. et al., 2004b, MNRAS, 356, 331
- Thomas, C.L. et al., 2004, astro-ph/0410341
- Udalski A., Zebruń K., Szymański, M., Kubiak M., Pietrzyński G., Soszyński I., Woźniak P. R. 2000, Acta Astronomica, 50, 1
- Udalski, A. et al. 1994, Acta Astronomica, 44, 165
- Udalski A. et al. 2002, Acta Astronomica, 52, 217
- Udalski A., Kubiak M., Szymański M. K., 1997, Acta Astronomica, 47, 319
- Udalski, A. 2003, Acta Astronomica, 53, 291
- Wood, A., & Mao, S. 2005, preprint (astro-ph/0507210)
- Woźniak P. R., & Paczyński, B. 1997, ApJ, 487, 55
- Woźniak P. R., 2000, Acta Astronomica, 50, 421
- Woźniak, P. R., et al. 2001, Acta Astronomica, 51, 175
- Zhao, H. & Mao, S. 1996, MNRAS, 283, 1197
- Zhao, H., Spergel, D. N. & Rich, R. 1995, ApJ, 440, L13



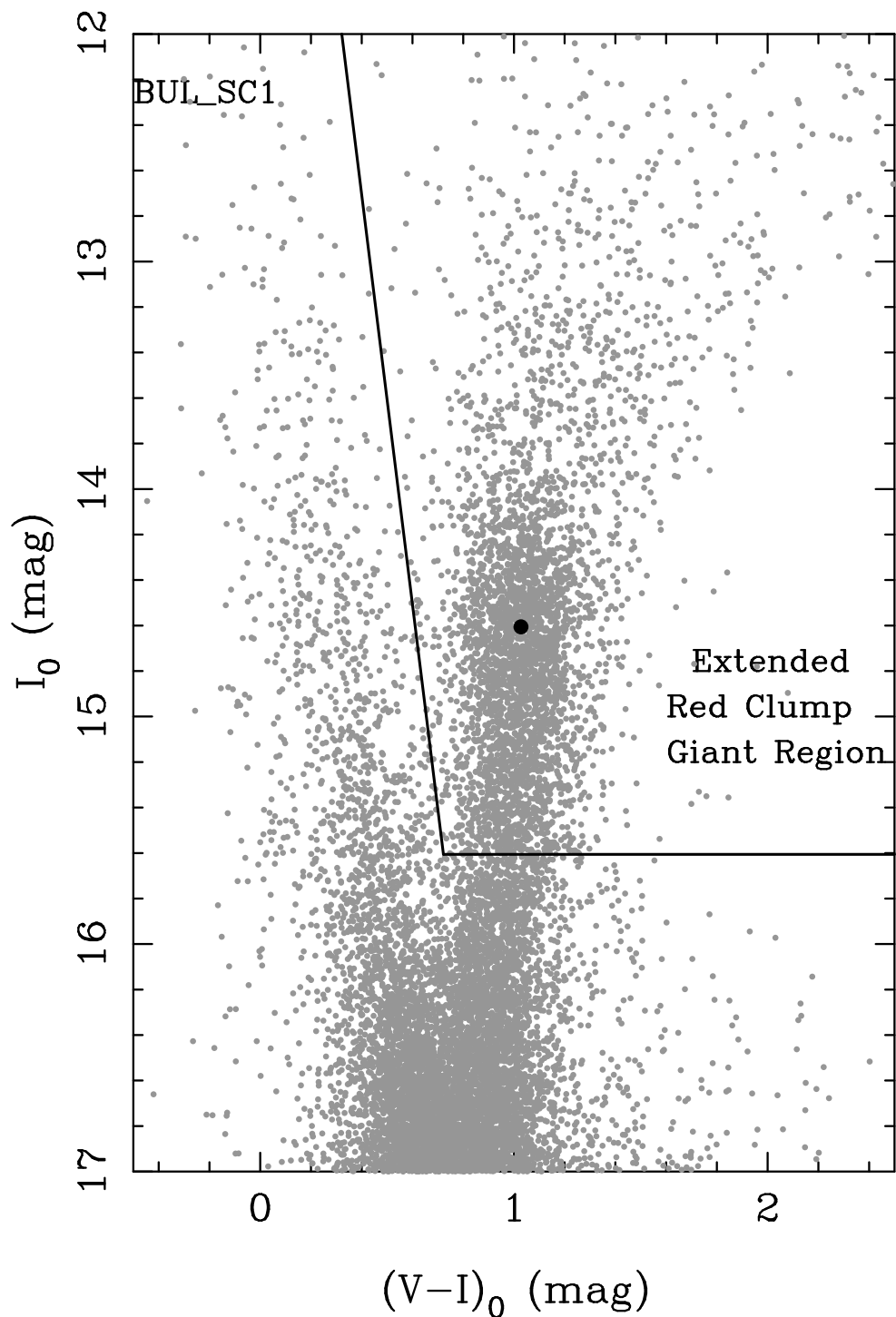


Fig. 1.—: Color Magnitude Diagram of the BUL\_SC1 field. Our extended RCG region is defined as the upper right portion of the figure with respect to the solid line. The filled circle represents the “center” of the RCG distribution from Sumi (2004).

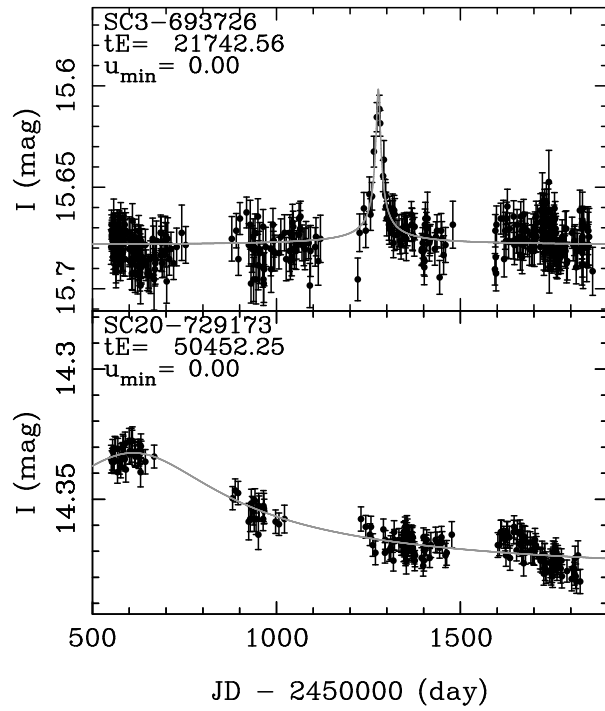


Fig. 2.—: Light curves of 2 sample events that were rejected by the condition  $t_E < 400$  d. The first object (top) has strongly degenerate and unreliable model parameters, and may represent an extreme case of blending. The second object (bottom) is likely a low amplitude variable star.

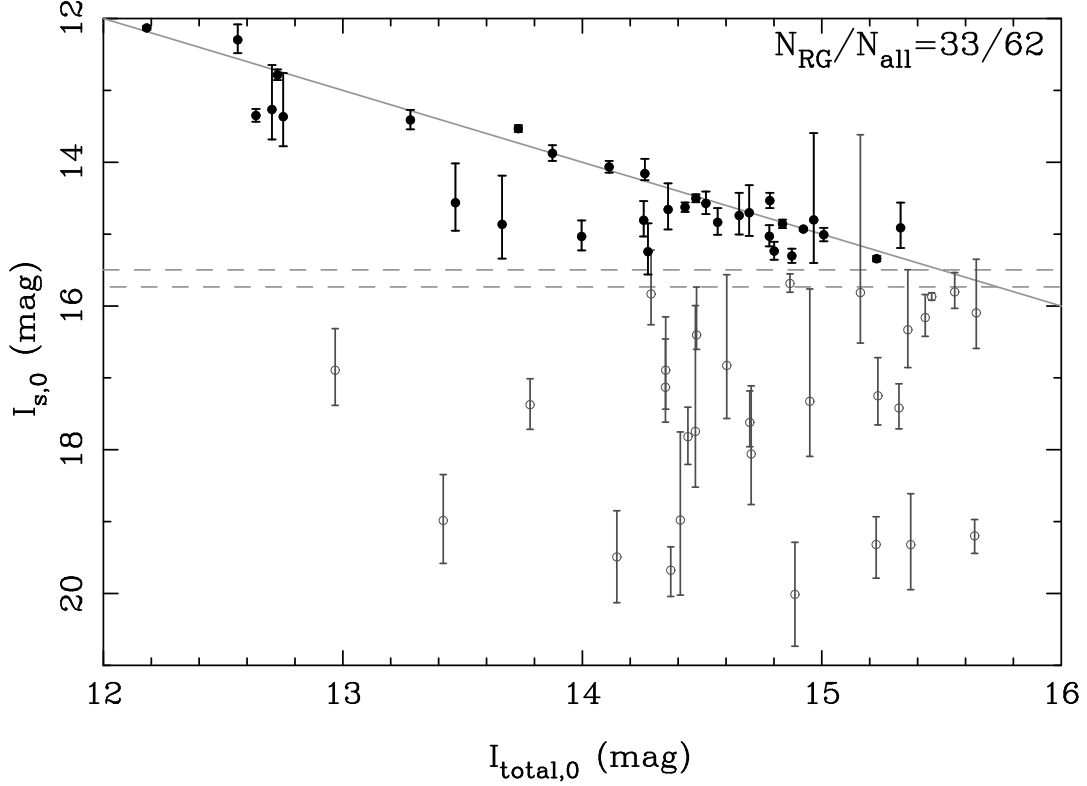


Fig. 3.—: Best fit source magnitude  $I_{s,0}$  versus the total baseline magnitude  $I_{\text{total},0}$  for 62 OGLE-II microlensing events. Magnitudes are corrected for extinction. Filled and open circles represent, respectively, sources above and below the threshold at  $I_{\text{RC,th}}$  (c.f. the final cut in Table 2). Solid line indicates  $I_{s,0} = I_{\text{total},0}$ , a blending free case. Dashed lines indicate the range of field dependent threshold  $I_{\text{RC,th}}$ .

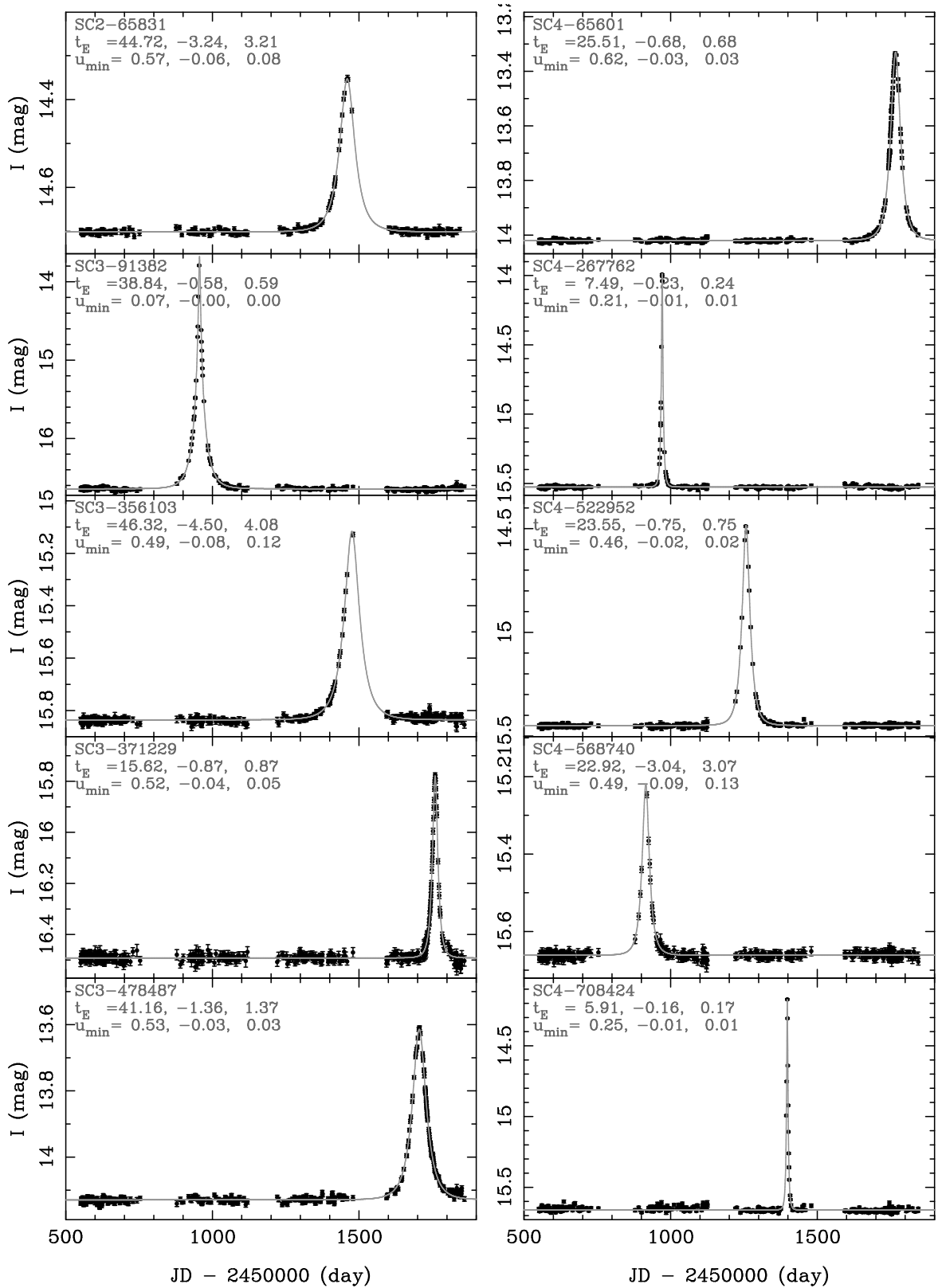


Fig. 4.—: Light curves of 33 level 6 events. This is our optical depth sample. Note that SC31-111306 and SC30-717699 are the same event. The field/star ID, as well as the best fit parameters  $t_E$  and  $u_{\min}$  with their 68% lower and upper confidence limits are also shown. For SC33-553617, the best fit parallax model is shown as dotted line.

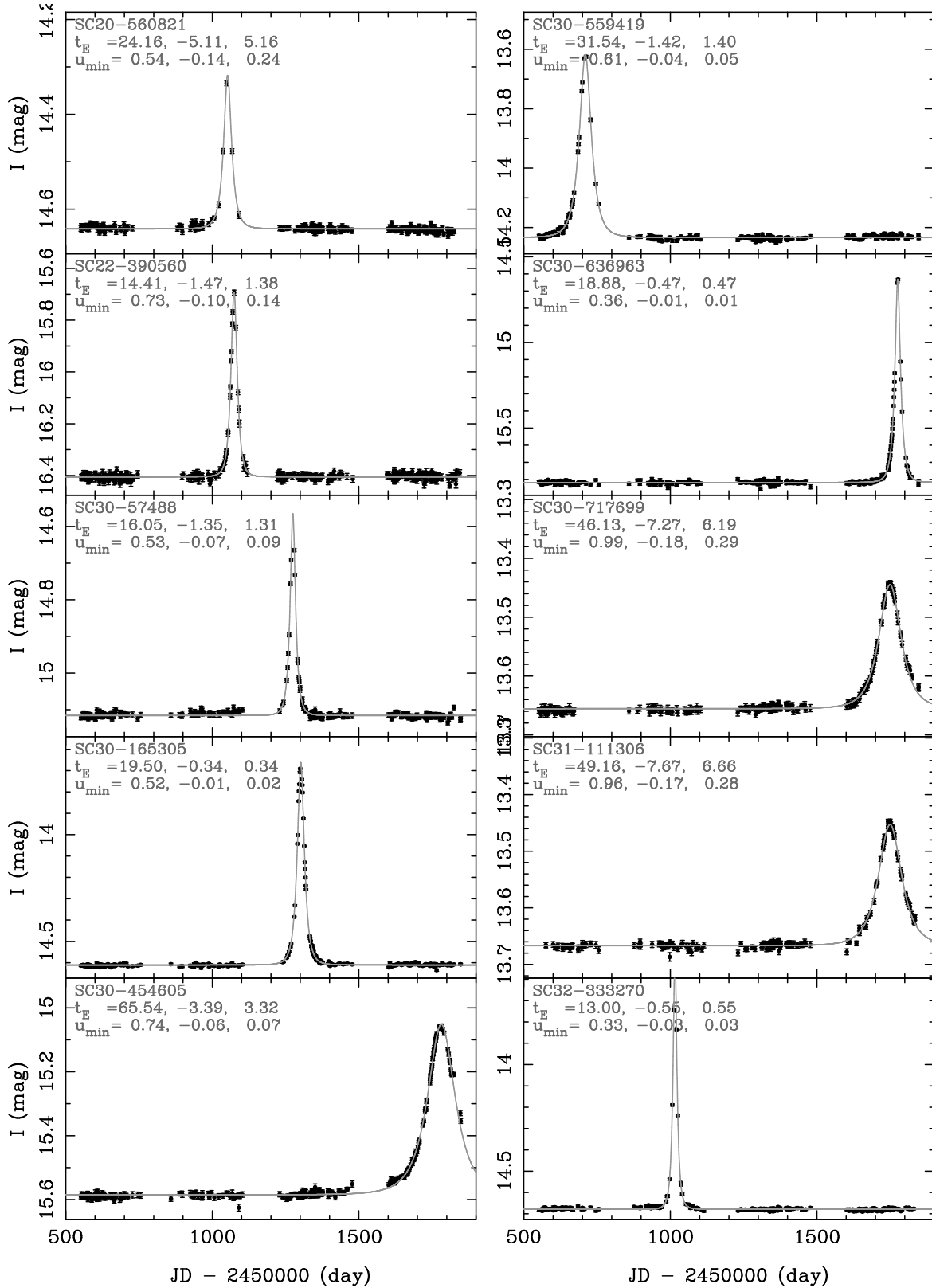


Fig. 4.—: continued.

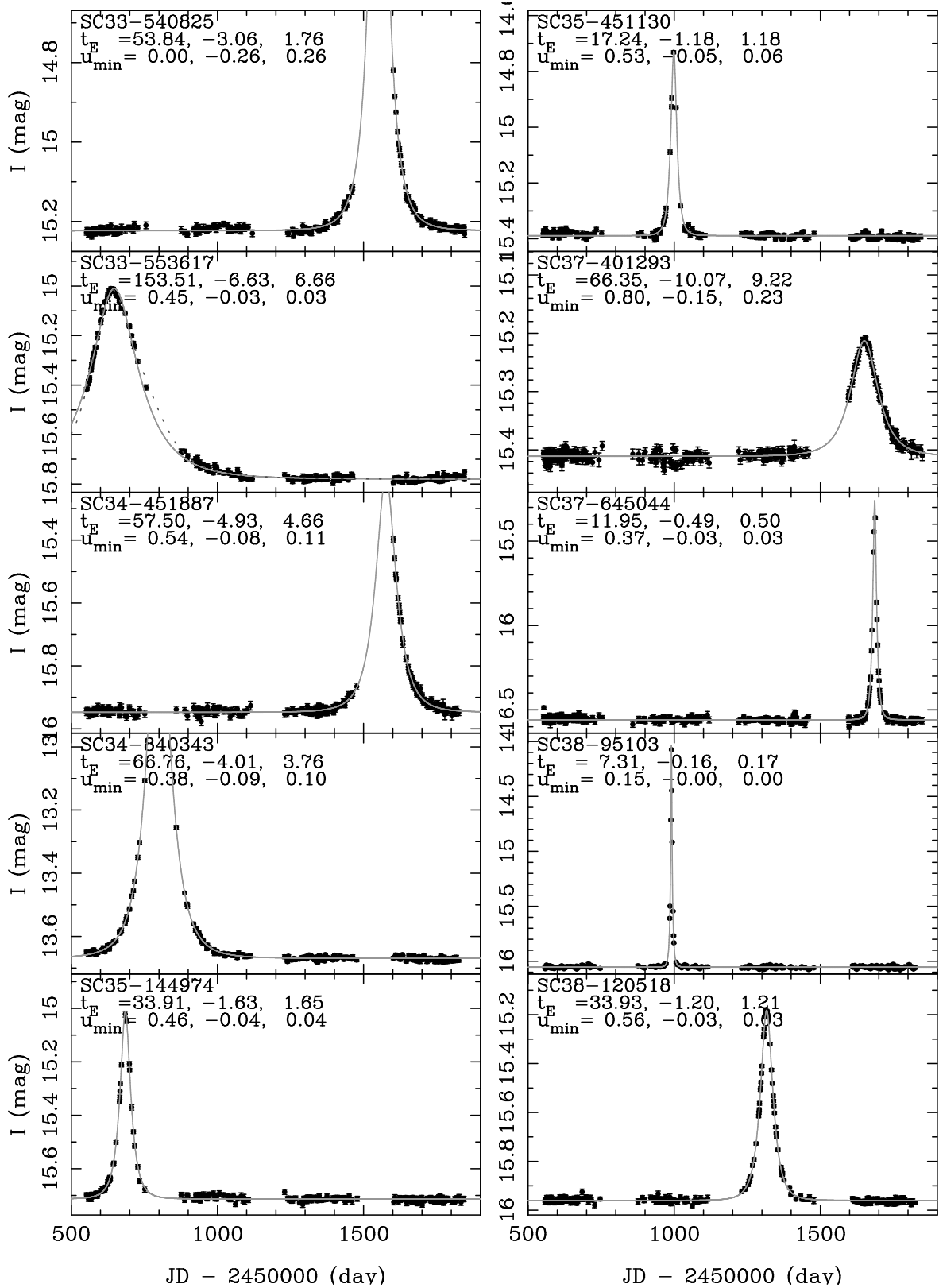


Fig. 4.—: continued.

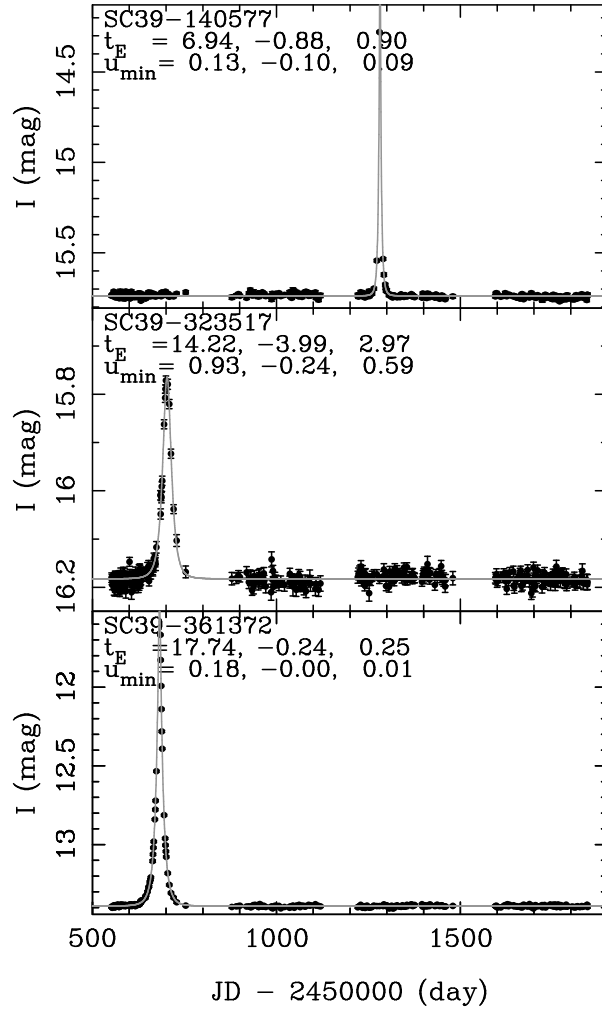


Fig. 4.—: continued.

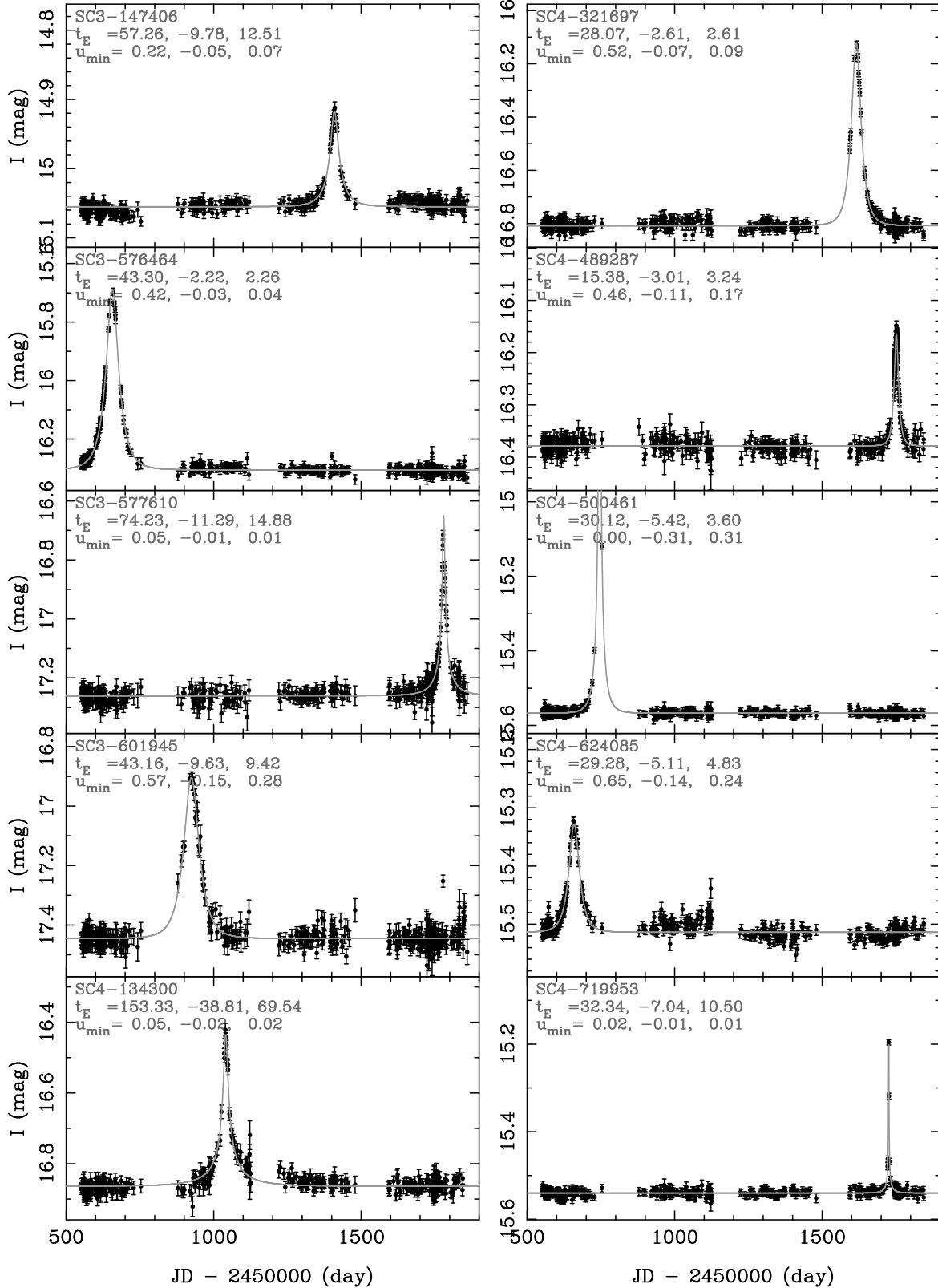


Fig. 5.—: Sample light curves of 10 level 5 events rejected for blending by level 6 criteria.



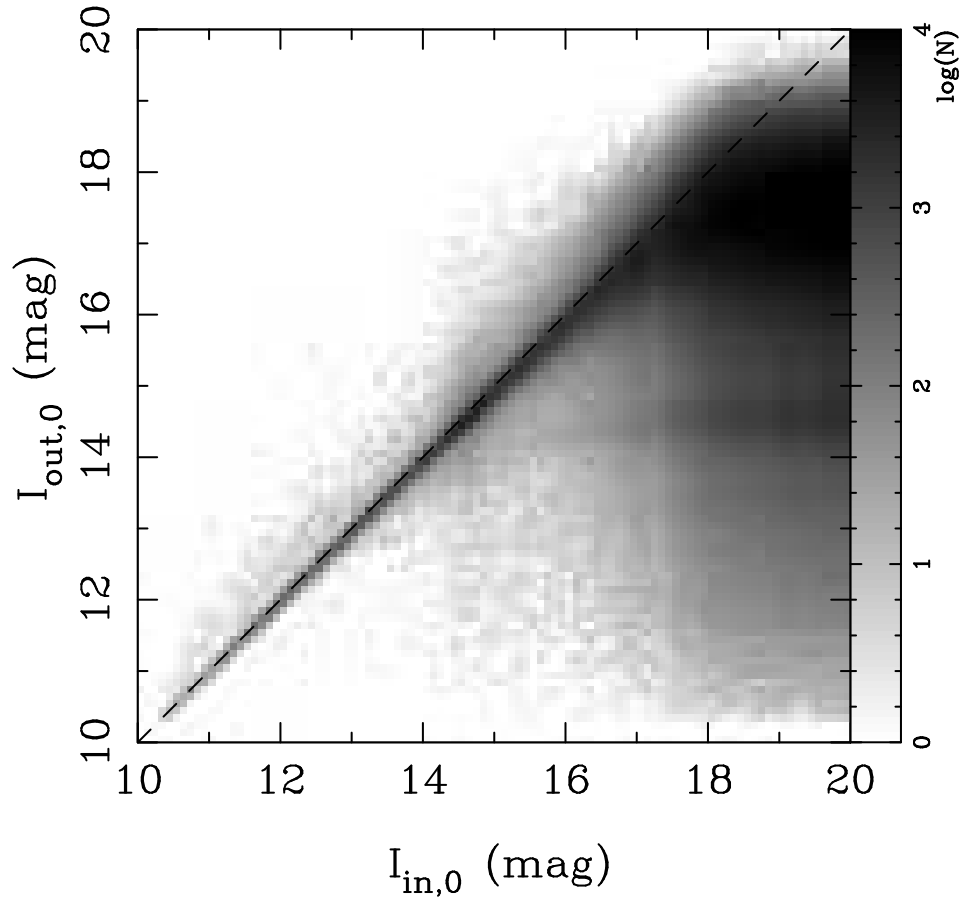


Fig. 6.—: Number density of the relation between the input ( $I_{\text{in},0}$ ) and the output ( $I_{\text{out},0}$ ) extinction corrected magnitudes simulated for BUL\_SC3 field. Source confusion intrinsic to the simulation is visible in a small fraction of detections located just above the diagonal line.

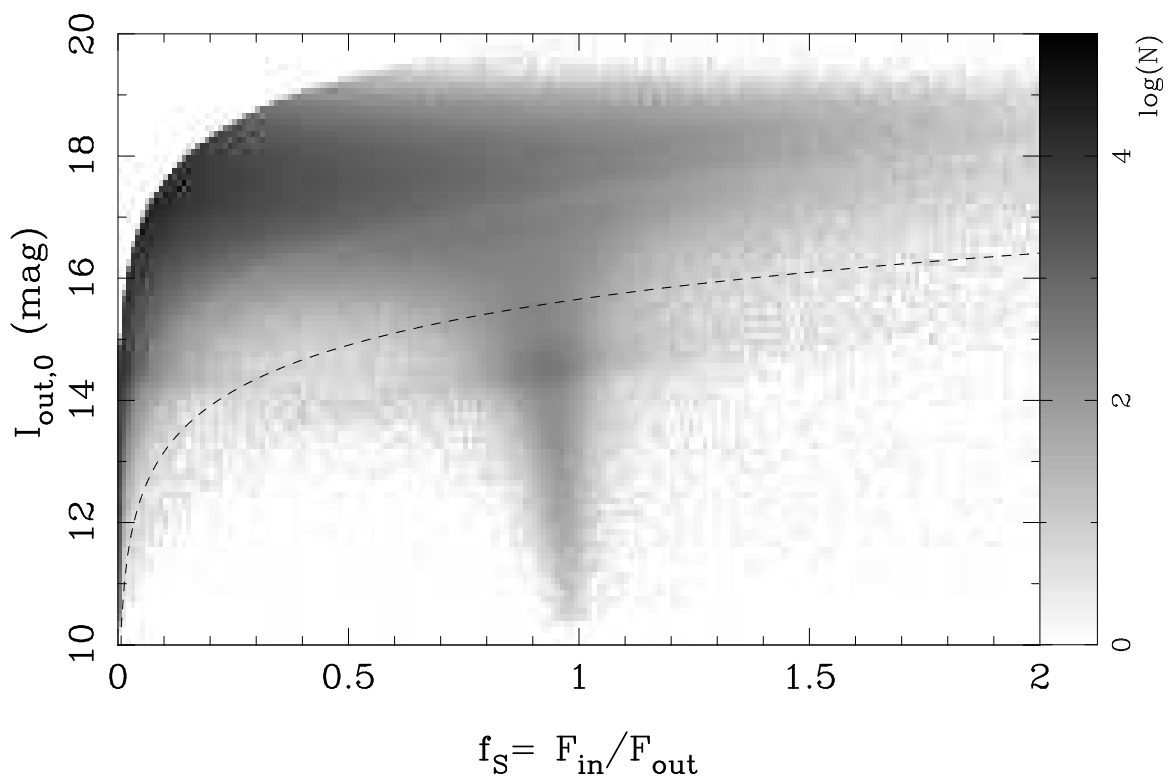


Fig. 7.—: Number density of the blending parameter  $f_S$  as a function of the extinction corrected output magnitude  $I_{\text{out},0}$  simulated for BUL\_SC3 field. The luminosity function is truncated for objects fainter than  $I_{\text{in},0} = 20$  mag. The area below the dashed line represents true sources brighter than the threshold:  $I_{\text{in},0} < I_{\text{RC,th}} = 15.66$  mag.

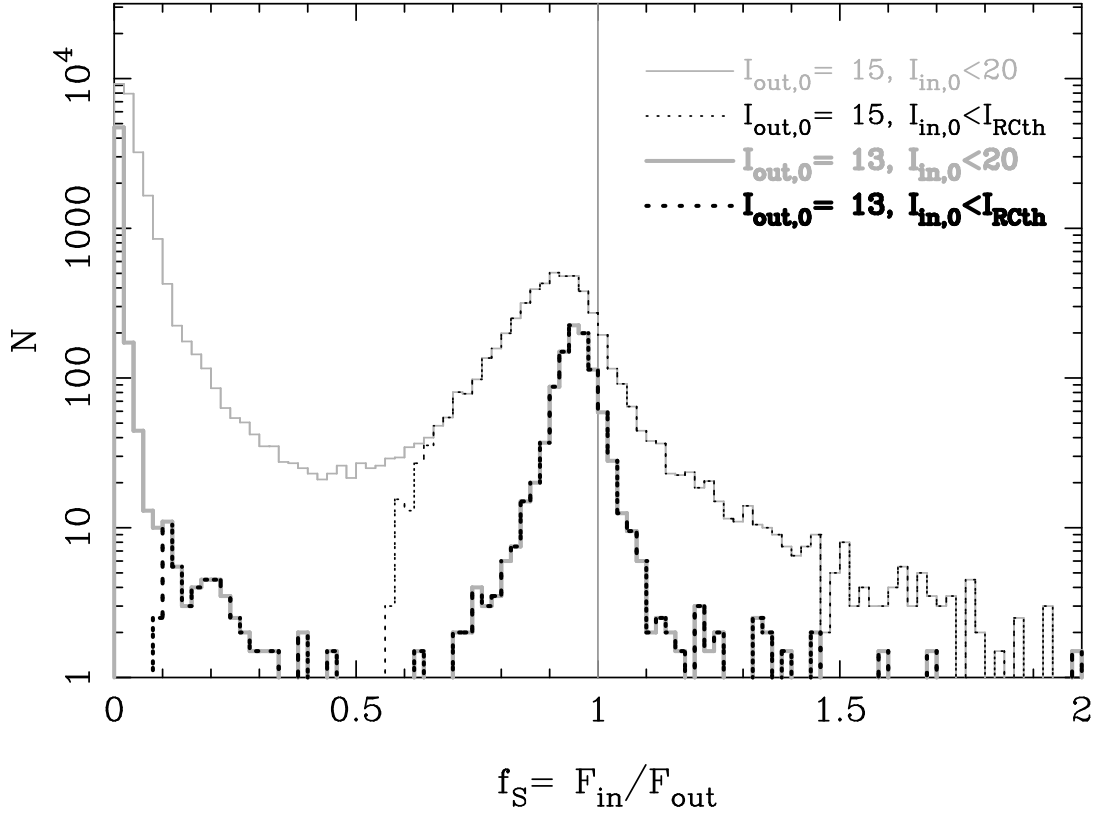


Fig. 8.—: Histograms of the blending parameter  $f_S$  in two narrow ranges of the extinction corrected output magnitude  $I_{\text{out},0}$ , as simulated for BUL\_SC3 field: 15 – 15.2 mag (thin lines) and 13 – 13.2 mag (thick lines). Solid and dashed lines are for  $I_{\text{in},0} < 20$  mag and  $I_{\text{in},0} < I_{\text{RC,th}} = 15.66$  mag, respectively.

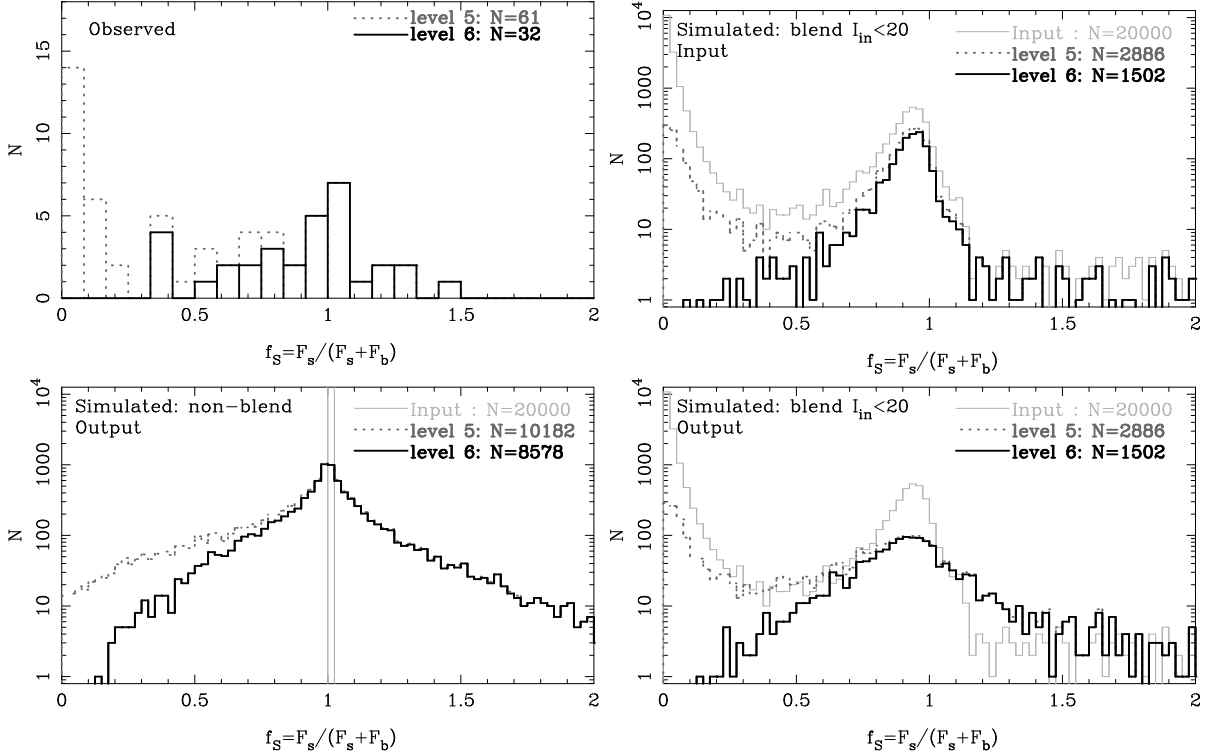


Fig. 9.—: Distributions of the blending parameter  $f_S$ . Solid lines are for level 6 events (optical depth sample), and dotted lines are for level 5 events (right before rejection of blends). Light gray lines in relevant panels represent simulated events before folding through light curve sampling efficiency (see § 4 for details). Top-left: observed samples. Top-right: “true” values used to generate simulated event samples ( $I_{\text{in}} < 20$  mag, compare Figs. 7 and 8). Bottom-left: best fit values (using a 5-parameter model with free  $f_S$ ) for simulated events without blending, i.e. generated from a curve with  $f_S \equiv 1$ . The results in this panel fully support our conclusion that the observed level 5 sample cannot be explained by a parent distribution with  $f_S = 1$ . We can see that  $\sim 16\%$  of unblended events failed the level 6 cut. Bottom-right: best fit values (using a 5-parameter model with free  $f_S$ ) for simulated events with blending, i.e. using input  $f_S$  distribution from image simulations. Those simulations are fully consistent with observations (Top-left panel) for both level 5 and 6 samples.

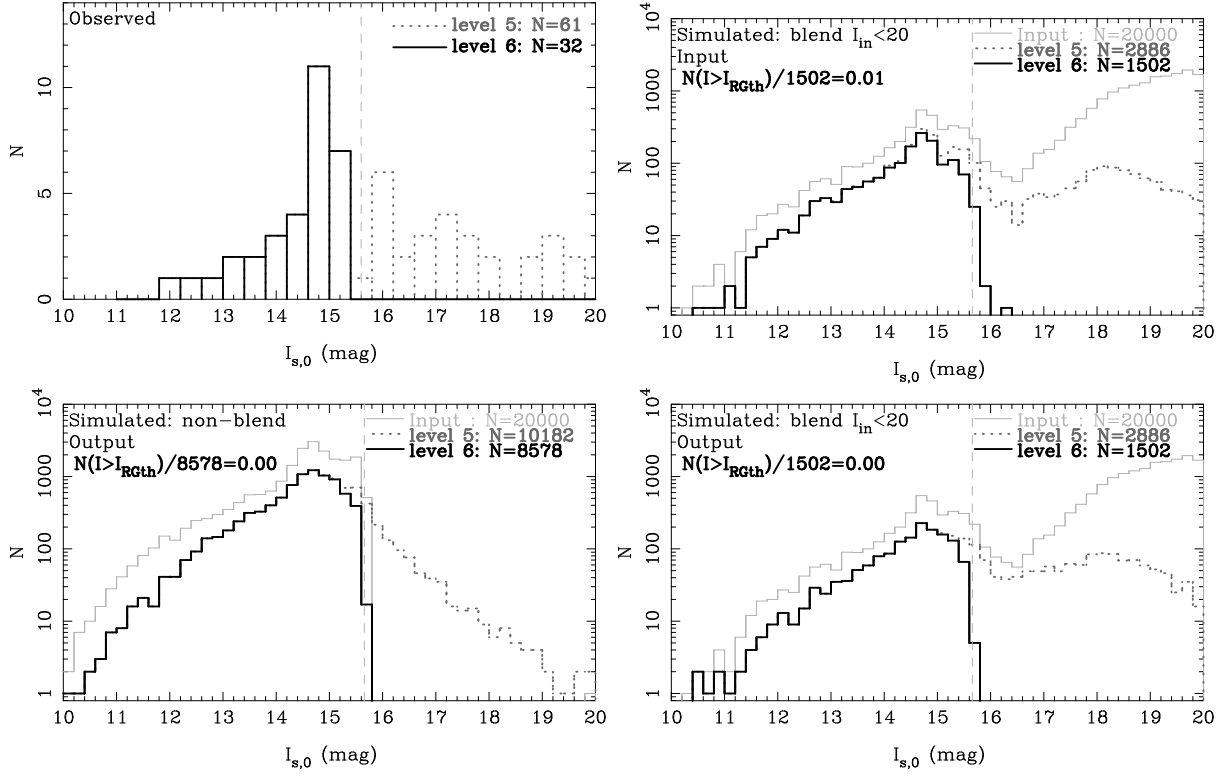


Fig. 10.—: Distributions of the extinction corrected source magnitude  $I_{s,0}$ . The assignment of samples to panels and line styles are the same as in Fig. 9. The dashed vertical line indicates the magnitude threshold  $I_{RC,th} = 15.6$  in BUL\_SC3 field. Only 1% of the simulated level 6 events originates from source stars below the threshold (top-right). The fraction of unblended events accidentally lost due to rejection of blends at level 6 is about 16% (bottom-left).

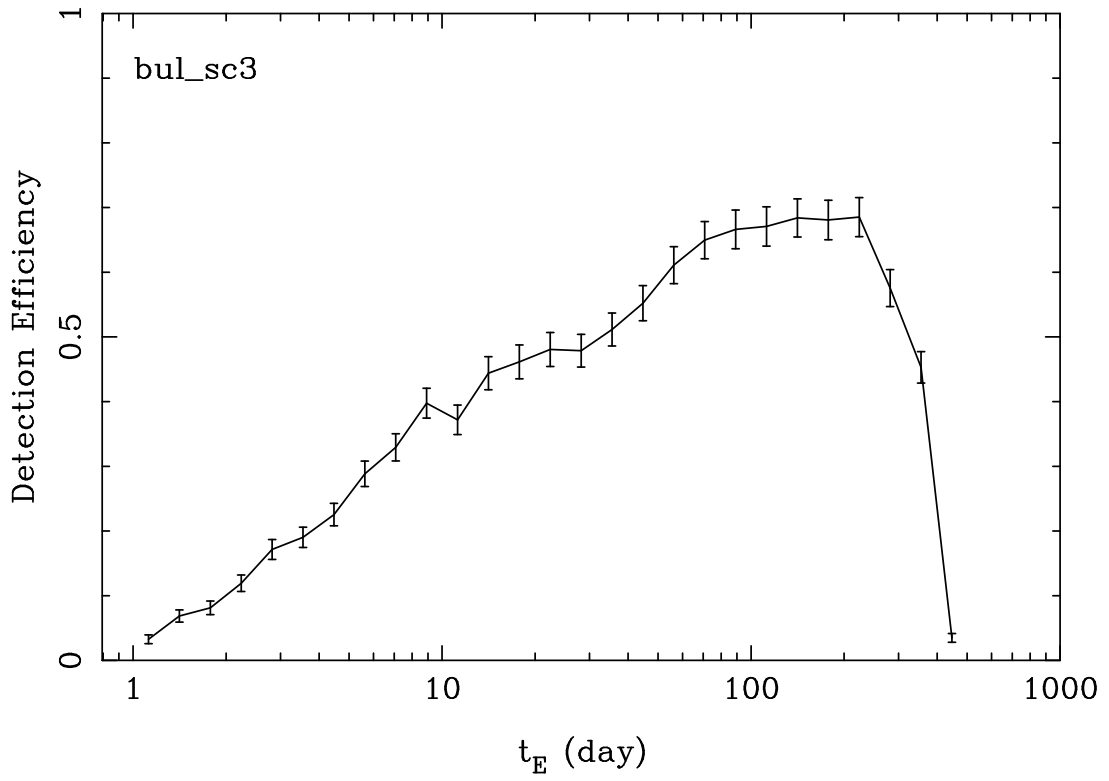


Fig. 11.—: OGLE-II microlensing detection efficiency as a function of  $t_E$  in BUL\_SC3 field.

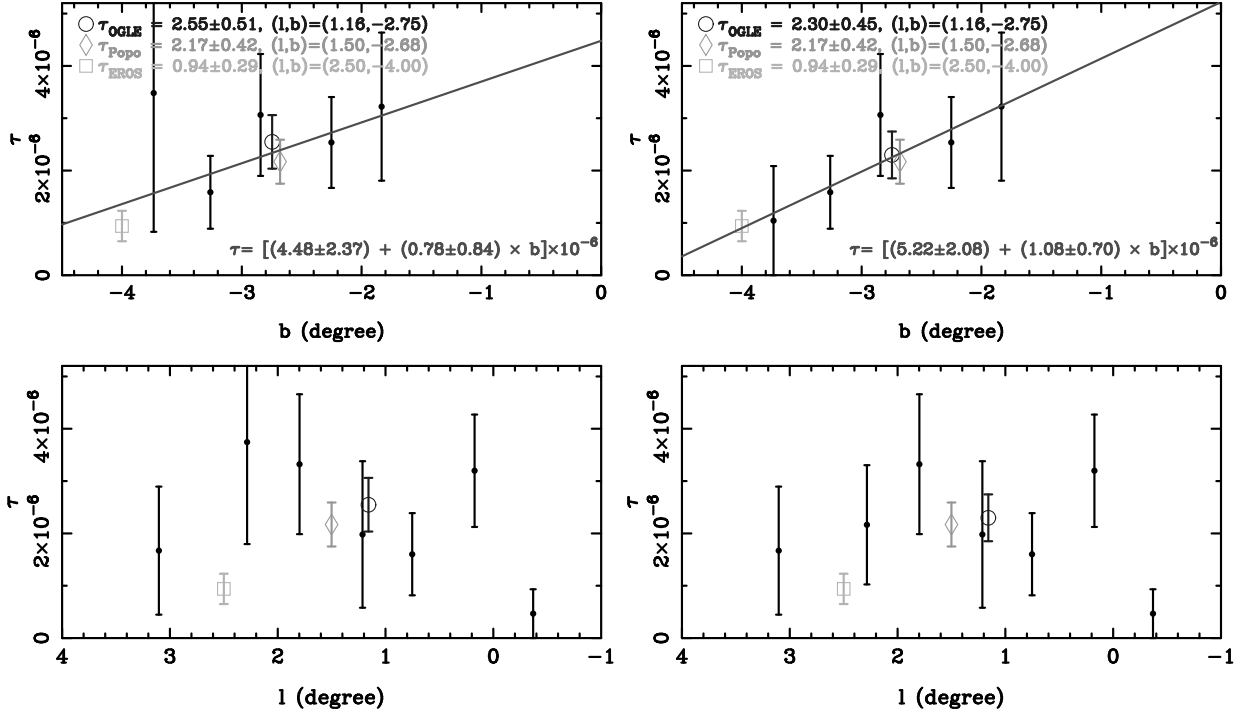


Fig. 12.—: Microlensing optical depth  $\tau$  as a function of the Galactic  $l$  and  $b$  (filled circles). The results based on the full level 6 sample from OGLE-II (left) are compared to the ones obtained after the parallax event has been removed (right). The latter case is a better representation of the bulge structure since the parallax event was likely caused by a disk lens. Also shown is the average  $\tau$  in all 20 fields weighted by the stellar number density (open circle). Solid line is the best fit linear gradient along  $b$ . There is no indication of gradient along  $l$  in this data. Open diamond and open square represent results from Popowski et al. (2004) and Afonso (2003).

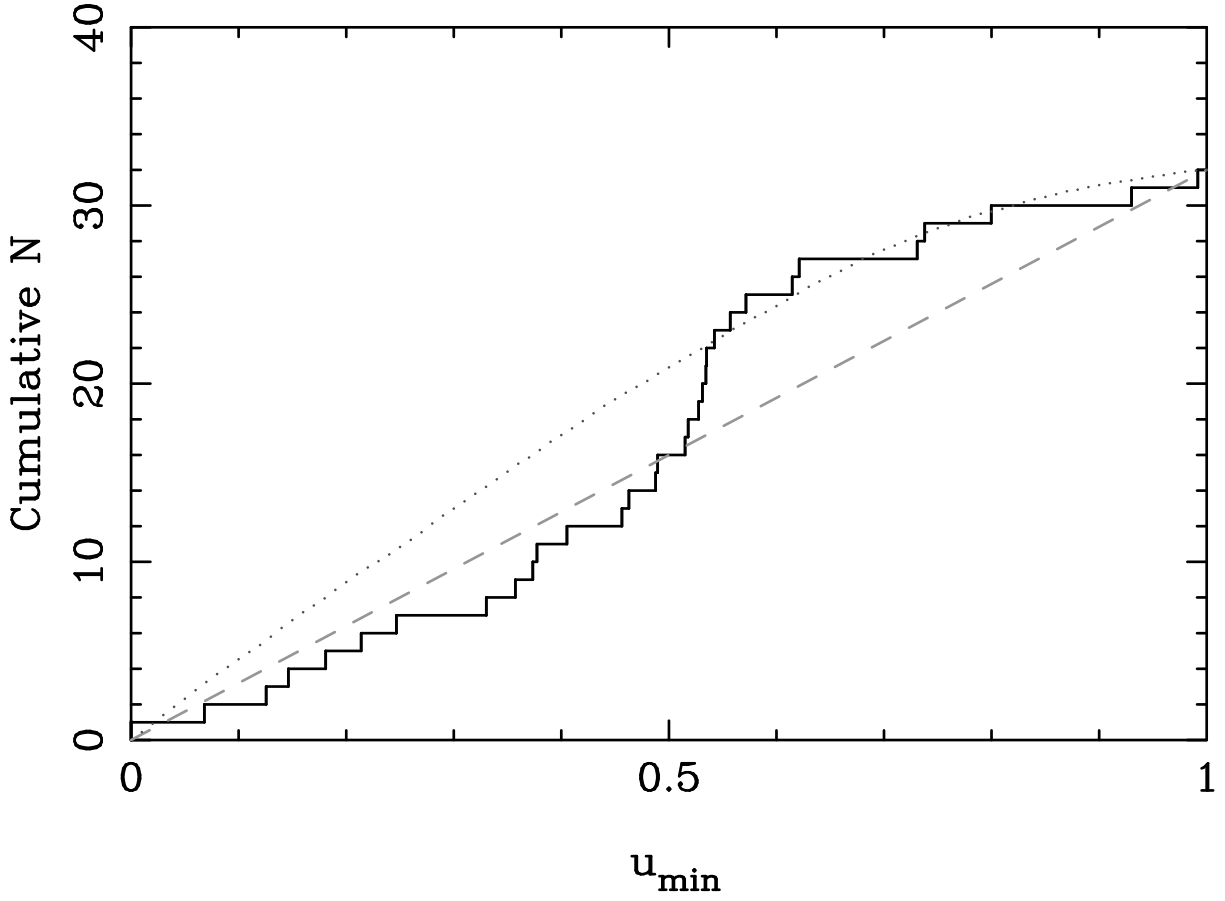


Fig. 13.—: Cumulative histogram of the best fit impact parameters  $u_{\min}$  for 33 events in the optical depth sample. For comparison we also show a flat distribution in  $u_{\min}$  (dashed line) and the expected distribution from Monte-Carlo simulations (dotted line).



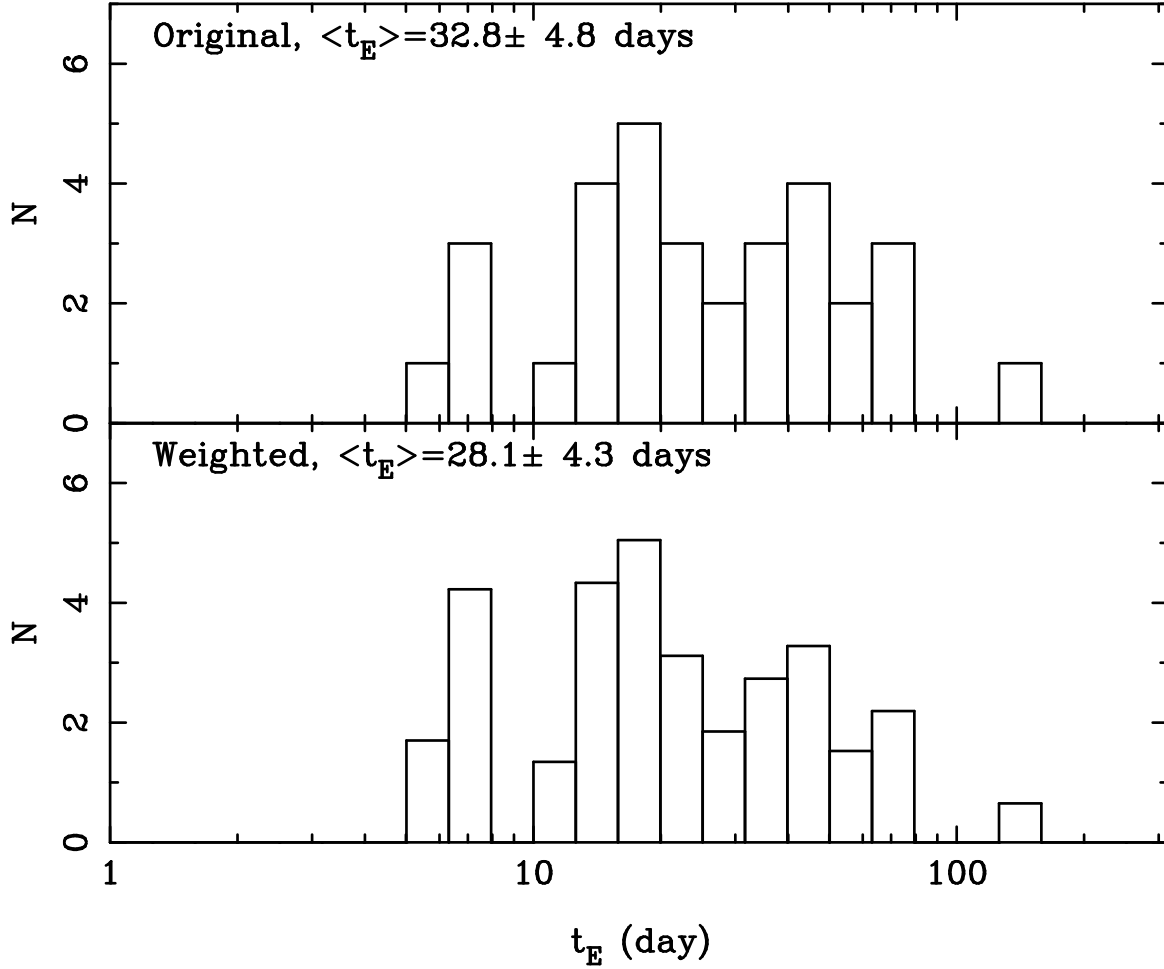


Fig. 14.—: Histogram of the best fit time-scale  $t_E$  for 32 events in the optical depth sample. The two distributions are: uncorrected for detection efficiency (top) and weighted by the inverse efficiency (bottom). The corrected mean time-scale  $\langle t_E \rangle = 28.1 \pm 4.3$  d is significantly longer than 14 d predicted by the current Galactic bar models without any streaming motions.

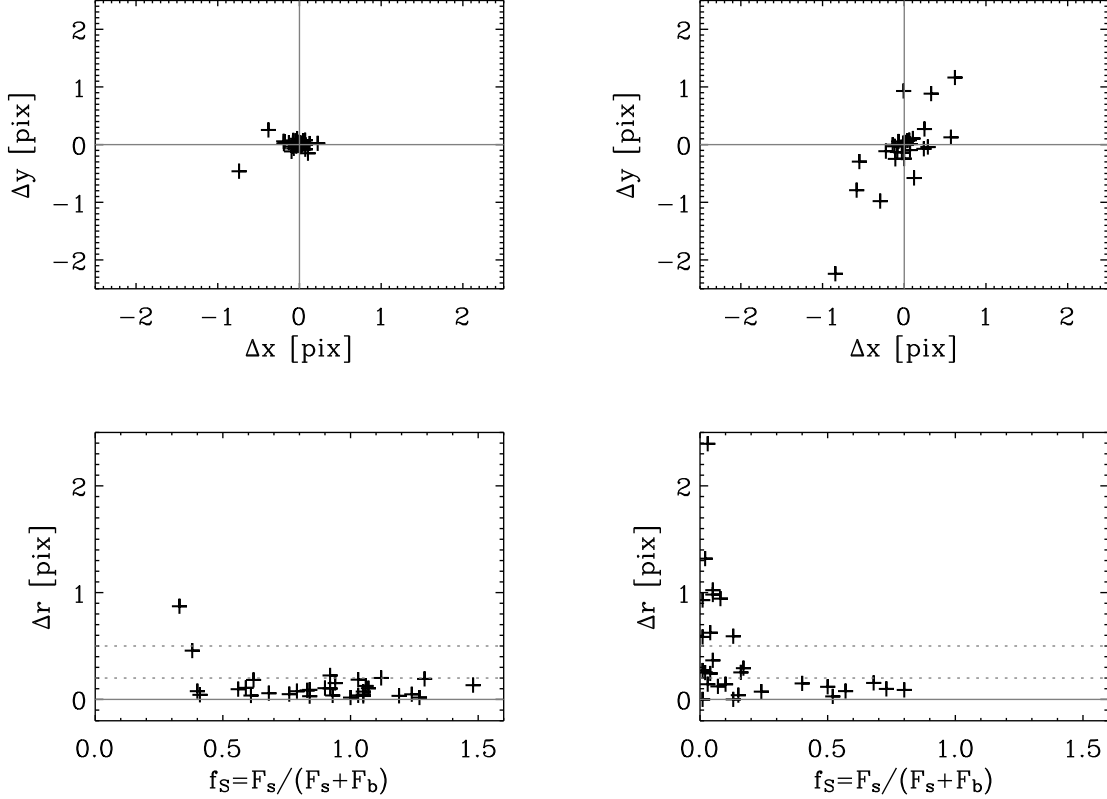


Fig. 15.—: Centroid shifts for microlensing events selected at level 6 (left) and level 5 events rejected for blending (right). The former sample is consistent with negligible blending, while in the full level 5 sample about one third of all sources shows a significant centroid shift. Top panels show differences in 2D source positions between the reference image, i.e. with low magnification, and a stack of difference images near the peak magnification. At the bottom we plot the total shift  $\Delta r$  versus the fitted fraction of the lensed light  $f_s$ . The fraction of significant centroid shifts agrees with predictions based on simulated images. Note that large shifts are only observed in strong “photometric blends” with low  $f_s$ .

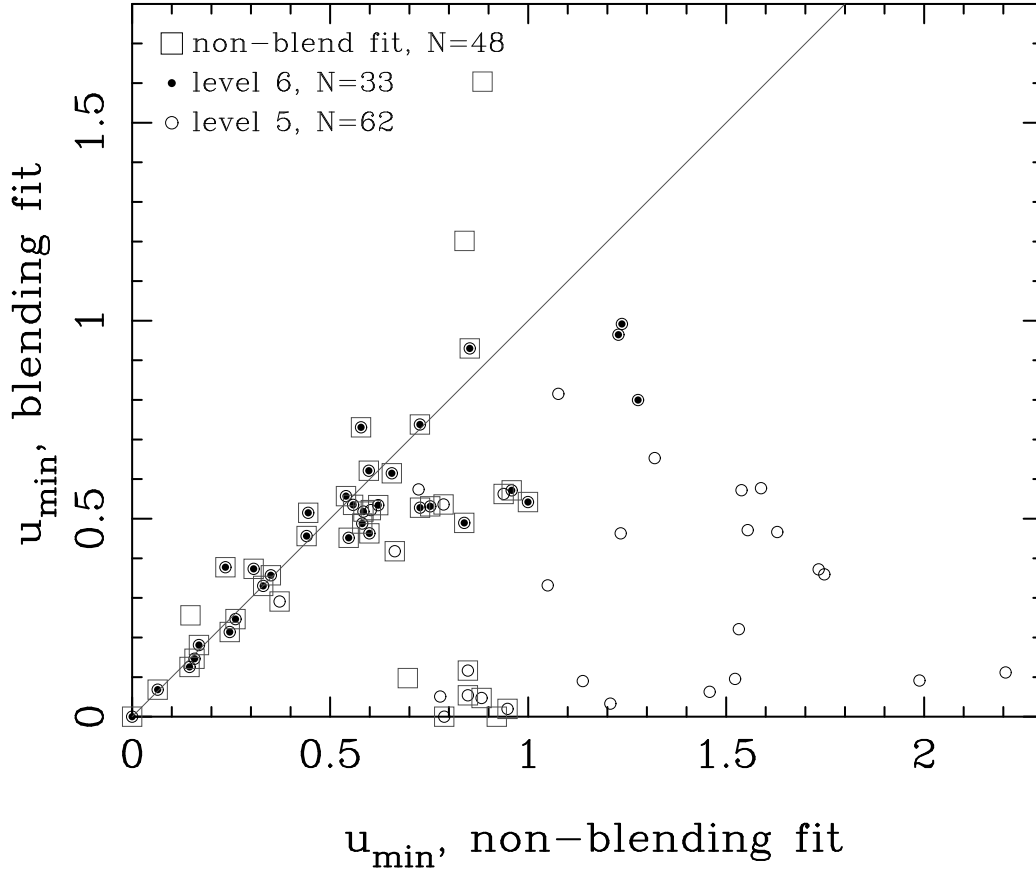


Fig. 16.—: Best fit impact parameter  $u_{\min}$  in microlensing models with and without blending. Compared are level 6 events (dots), level 5 events (open circles) and our control sample (open squares). Three open squares fall outside the figure area with  $u_{\min}$  reaching 16. Fitting a  $f_S = 1$  model to significantly blended events results in overestimated  $u_{\min}$ .

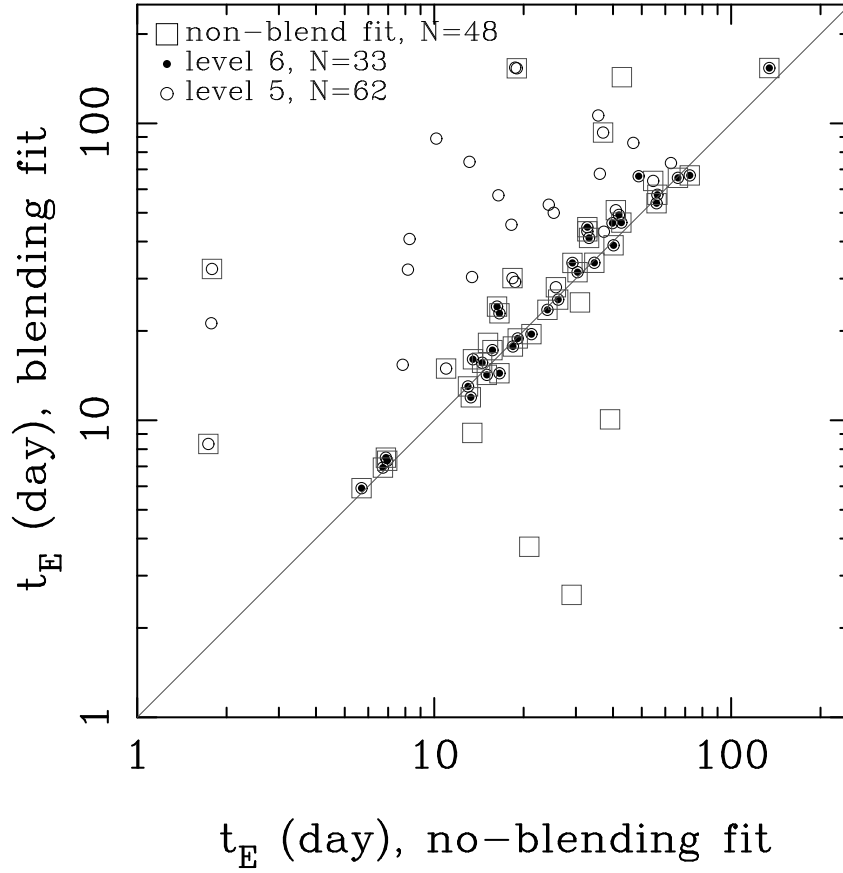


Fig. 17.—: Best fit time-scale  $t_E$  in microlensing models with and without blending. Symbols are the same as in Fig. 16. One open square falls outside the figure area with  $t_E = (3.4 \pm 3.4) \times 10^4$  d. Fitting a  $f_S = 1$  model to significantly blended events results in underestimated  $t_E$ .

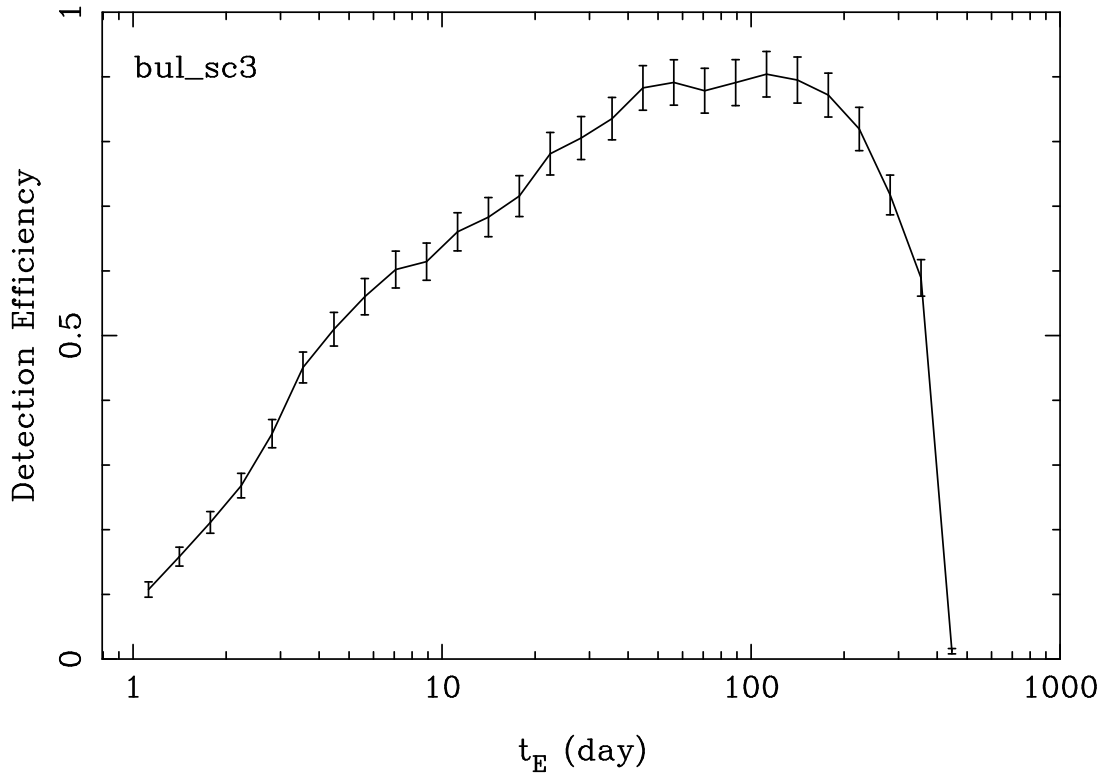


Fig. 18.— OGLE-II microlensing detection efficiency assuming no blending in the RCG sample (BUL\_SC3). Our data are inconsistent with that assumption. This curve is shown only for the purpose of comparing our present analysis with previously published work.

Table 1. OGLE-II GB fields contributing to the present optical depth analysis. Also given are Galactic coordinates of the field center ( $l$ ,  $b$ ), number of source stars ( $N_s$ ), number of microlensing events ( $N_{\text{lens}}$ ), optical depth ( $\tau$ ) and its error ( $\sigma_\tau$ ).

Field	$l$ ( $^\circ$ )	$b$ ( $^\circ$ )	$N_s$	$N_{\text{lens}}$	$\tau(10^{-6})$	$\sigma_\tau(10^{-6})$
1	1.08	-3.62	35844	0	0.000000	0.000000
2	2.23	-3.46	38278	1	2.483758	2.483758
3	0.11	-1.93	80976	4	4.286616	2.226285
4	0.43	-2.01	78454	5	3.145996	1.494732
20	1.68	-2.47	58891	1	1.239517	1.239517
21	1.80	-2.66	52930	0	0.000000	0.000000
22	-0.26	-2.95	50732	1	0.854807	0.854807
23	-0.50	-3.36	42205	0	0.000000	0.000000
30	1.94	-2.84	47974	6	9.543987	4.183375
31	2.23	-2.94	45825	1	2.261020	2.261020
32	2.34	-3.14	40476	1	0.937948	0.937948
33	2.35	-3.66	34461	2	10.415521	7.933656
34	1.35	-2.40	61515	2	4.087111	2.890040
35	3.05	-3.00	41146	2	3.211394	2.350345
36	3.16	-3.20	37922	0	0.000000	0.000000
37	0.00	-1.74	85289	2	2.211746	1.772319
38	0.97	-3.42	40148	2	2.876526	2.246087
39	0.53	-2.21	72842	3	1.621968	0.967699
45	0.98	-3.94	32823	0	0.000000	0.000000
46	1.09	-4.14	29626	0	0.000000	0.000000

Table 2. Selection criteria for microlensing events. The last column gives the number of candidate events passed to the next level.

Level	Criteria	$N_{\text{cand}}$
0	$I_0 < 9 \times (V - I)_0 + I_{\text{RC},0} - 5.5$ $I_0 < I_{\text{RC},\text{th}}$ $N_{\text{data}} \geq 70$	1,084,267
1	$0 < N_{\text{peak}} < 4$ $\sigma_{\text{max}} \geq 6$ $\sum_{\text{peak,max}} \sigma_i \geq 20$ $\chi_{\text{out}}^2 / d.o.f < 2.2$ for $\sigma_{\text{max}} < 10$	821
2	$530 \leq t_0 \leq 1860$ $t_E \leq 400$ d $u_{\text{min}} < 1$ $\chi_{\text{ml}}^2 \leq 1.0$ for $\sigma_{\text{max}} < 7.5$ $\chi_{\text{ml}}^2 \leq 1.5$ for $7.5 \leq \sigma_{\text{max}} < 10$ $\chi_{\text{ml}}^2 \leq 1.8$ for $10 \leq \sigma_{\text{max}} < 30$	135
3	reject spurious events	81
4	error estimates converged for all parameters	69
5	$\chi_{\text{ml}}^2 \leq 3.5$ and no cross ref with binary events	62
6	$I_{\text{s},0} + \sigma_{I_{\text{s}+}} < I_{\text{RC},\text{th}}$	33

Table 3. Binary lens events cross-referenced with other samples.

ID <sub>OGL</sub>	ID <sub>Ref</sub>	Reference
SC20-395103	401.48408.649 or 98-BLG-14	Alcock et al. (2000a)
SC30-352272	108.19333.1878 or 108-E	Alcock et al. (2000a)
SC21-45456	113.18674.756 or 97-BLG-1	Alcock et al. (2000a)
SC20-69068	sc20-1793	Jaroszynski (2002)

Table 4. Microlensing events used in the optical depth measurement (after the final level 6 cut). Only 32 events are unique due to a duplicate event in the overlap region between two fields: SC31-111306 and SC30-717699.

Field-ID	R.A.	Dec.	$\sigma_{\max}$	$t_0$	$t_E$	$u_{\min}$	$f_S$	$I_{s,0}$	$\frac{\chi^2}{dof}$
SC2-65831	18:04:06.85	-29:01:17.2	57	1459.9±0.4	44.7±3.1	0.572 ±0.066	0.40±0.07	15.0±0.2	0.56
SC3-91382	17:53:09.33	-30:01:12.1	135	956.0±0.0	38.8±0.6	0.068 ±0.002	1.05±0.02	14.9±0.0	0.95
SC3-356103	17:53:33.93	-29:46:15.6	54	1475.8±1.0	46.3±4.2	0.488 ±0.095	0.76±0.22	14.7±0.3	0.90
SC3-371229	17:53:21.13	-29:40:37.4	49	1759.6±0.1	15.6±0.9	0.518 ±0.046	0.83±0.11	15.0±0.1	0.76
SC3-478487	17:53:47.38	-30:05:26.2	56	1705.5±0.1	41.2±1.4	0.531 ±0.029	0.56±0.05	13.4±0.1	1.64
SC4-65601	17:54:09.41	-29:53:36.9	111	1767.1±0.0	25.5±0.7	0.621 ±0.026	1.06±0.07	12.8±0.1	0.60
SC4-267762	17:54:21.79	-29:53:24.0	147	971.1±0.0	7.5±0.2	0.214 ±0.011	0.84±0.05	14.6±0.1	1.03
SC4-522952	17:54:38.64	-29:33:12.8	121	1257.1±0.1	23.6±0.7	0.456 ±0.024	1.05±0.08	14.1±0.1	0.55
SC4-568740	17:54:49.35	-29:20:25.0	39	915.2±0.2	22.9±3.0	0.490 ±0.108	0.41±0.13	15.2±0.4	0.53
SC4-708424	17:55:00.07	-29:35:03.7	126	1397.8±0.0	5.9±0.2	0.247 ±0.010	0.93±0.05	14.5±0.1	2.35
SC20-560821	17:59:27.19	-28:32:31.5	42	1052.2±0.3	24.2±5.2	0.542 ±0.183	0.33±0.17	14.9±0.6	1.01
SC22-390560	17:56:56.81	-31:11:51.0	48	1074.3±0.1	14.4±1.4	0.731 ±0.122	1.48±0.43	14.9±0.3	0.70
SC30-57488	18:01:02.52	-29:00:11.6	64	1274.8±0.1	16.0±1.3	0.528 ±0.082	0.61±0.14	14.8±0.2	0.98
SC30-165305	18:01:07.74	-28:31:41.7	155	1302.0±0.0	19.5±0.3	0.515 ±0.015	1.24±0.05	13.5±0.0	1.61
SC30-454605	18:01:30.89	-28:59:26.7	61	1781.4±0.2	65.5±3.1	0.738 ±0.056	1.03±0.14	14.6±0.2	1.35
SC30-559419	18:01:33.95	-28:28:02.3	81	709.9±0.2	31.5±1.4	0.615 ±0.047	0.90±0.11	13.4±0.1	1.62
SC30-636963	18:01:44.80	-28:58:03.5	113	1775.7±0.0	18.9±0.5	0.357 ±0.015	1.03±0.06	14.9±0.1	0.84
SC30-717699	18:01:52.15	-28:32:36.5	38	1749.3±0.3	46.1±6.6	0.992 ±0.217	0.62±0.28	13.3±0.5	0.76
SC31-111306	18:01:52.14	-28:32:36.5	36	1749.6±0.3	49.2±7.1	0.965 ±0.211	0.59±0.26	13.4±0.5	0.96
SC32-333270	18:03:21.74	-28:28:50.4	108	1015.8±0.0	13.0±0.5	0.330 ±0.031	1.00±0.10	13.9±0.1	1.07
SC33-540825	18:05:45.79	-28:30:52.4	45	1552.0±0.5	53.8±1.7	0.000 ±0.273	1.12±0.10	14.2±0.1	0.85
SC33-553617	18:05:46.71	-28:25:32.1	74	647.1±0.3	153.5±6.7	0.452 ±0.028	0.75±0.07	15.3±0.1	2.76
SC33-553617 <sup>a</sup>	–	–	–	668.3±1.1	140.9±16.4	0.405 ±0.101	0.84±0.26	15.2±0.4	1.21
SC34-451887	17:58:14.20	-28:48:22.3	45	1576.3±1.5	57.5±4.9	0.535 ±0.098	0.94±0.25	14.7±0.3	0.78
SC34-840343	17:58:37.12	-29:06:29.9	62	798.9±0.3	66.8±3.9	0.377 ±0.096	1.29±0.24	12.3±0.2	0.95
SC35-144974	18:04:09.65	-27:44:34.9	54	684.9±0.1	33.9±1.6	0.463 ±0.038	0.68±0.08	15.2±0.1	0.85
SC35-451130	18:04:33.63	-28:07:32.2	68	998.6±0.1	17.2±1.1	0.534 ±0.057	0.79±0.13	14.8±0.2	1.61
SC37-401293	17:52:32.30	-29:58:46.8	22	1650.3±0.5	66.3±9.5	0.800 ±0.179	0.38±0.16	14.6±0.5	0.82
SC37-645044	17:52:58.69	-29:34:22.2	78	1685.7±0.0	12.0±0.5	0.373 ±0.029	1.27±0.13	14.5±0.1	0.91
SC38-95103	18:01:09.74	-29:56:18.9	197	990.5±0.0	7.3±0.2	0.146 ±0.005	0.92±0.03	15.3±0.0	1.00
SC38-120518	18:01:10.23	-29:48:55.2	88	1316.1±0.1	33.9±1.2	0.557 ±0.031	1.05±0.09	15.0±0.1	0.79
SC39-140577	17:55:17.08	-29:37:41.0	150	1281.4±0.1	6.9±0.9	0.126 ±0.083	0.92±0.29	14.7±0.4	1.11
SC39-323517	17:55:36.42	-29:42:14.0	29	702.7±0.2	14.2±3.3	0.930 ±0.333	1.19±0.85	14.8±0.9	0.89
SC39-361372	17:55:28.67	-29:33:41.7	154	682.3±0.0	17.7±0.2	0.181 ±0.005	1.07±0.03	12.1±0.0	0.65

Note. — The symmetric 68% confidence intervals shown here are only for the purpose of quick reference and avoiding a large amount of unnecessary details. The analysis is based on proper asymmetric confidence intervals. Complete information is available electronically at ApJ web.

<sup>a</sup>Parallax model fit with  $\psi = 3.17 \pm 0.12$  radian and  $\tilde{r}_E = 6.16 \pm 0.39$  AU.



Table 5. Microlensing events with evidence for faint blended sources. Those 29 events were rejected from the optical depth sample at level 6.

Field-ID	R.A.	Dec.	$\sigma_{\max}$	$t_0$	$t_E$	$u_{\min}$	$f_S$	$I_{s,0}$	$\frac{\chi^2}{dof}$
SC3-147406	17:53:09.61	−29:46:39.3	14	1409.2±0.4	57.3±10.6	0.221 ±0.058	0.04±0.01	17.4±0.4	1.20
SC3-576464	17:53:41.56	−29:39:06.0	40	656.5±0.2	43.3±2.2	0.418 ±0.035	0.50±0.06	15.7±0.1	0.76
SC3-577610	17:53:36.20	−29:38:08.2	23	1779.7±0.1	74.2±13.3	0.051 ±0.012	0.04±0.01	19.2±0.2	0.69
SC3-601945	17:53:36.63	−29:31:21.2	17	924.4±0.5	43.2±9.3	0.574 ±0.193	0.68±0.36	16.1±0.6	1.05
SC4-134300	17:54:13.04	−29:35:14.1	21	1041.0±0.2	153.3±50.0	0.047 ±0.018	0.02±0.01	19.3±0.4	0.82
SC4-321697	17:54:25.13	−29:37:49.4	36	1615.6±0.2	28.1±2.5	0.522 ±0.075	0.80±0.17	15.8±0.2	0.77
SC4-489287	17:54:42.92	−29:44:12.1	15	1751.5±0.1	15.4±3.1	0.463 ±0.130	0.16±0.07	17.2±0.5	0.80
SC4-500461	17:54:41.53	−29:40:10.1	41	745.8±0.3	30.1±3.5	0.000 ±0.232	0.17±0.03	16.4±0.4	0.53
SC4-624085	17:55:00.19	−29:59:53.6	14	659.3±0.3	29.3±4.1	0.653 ±0.149	0.24±0.09	15.8±0.5	1.73
SC4-719953	17:54:56.68	−29:31:47.6	37	1725.8±0.1	32.3±8.2	0.020 ±0.006	0.01±0.00	19.7±0.3	0.66
SC20-525747	17:59:28.45	−28:42:53.3	14	1746.3±0.2	5.3±3.9	0.063 ±0.140	0.02±0.02	19.0±1.1	0.66
SC21-766993	18:00:39.38	−28:55:14.6	28	1119.6±1.5	93.2±16.3	0.116 ±0.047	0.07±0.02	17.6±0.4	0.68
SC22-380074	17:56:58.83	−31:14:05.6	16	587.2±0.4	40.8±16.7	0.090 ±0.053	0.03±0.02	19.3±0.7	0.74
SC22-414328	17:56:59.20	−31:03:22.3	31	1832.8±0.6	51.0±5.1	0.536 ±0.092	0.52±0.14	16.2±0.3	0.62
SC23-524386	17:57:56.24	−30:51:58.9	82	1434.8±0.1	64.0±1.6	0.291 ±0.011	0.73±0.03	15.9±0.1	1.02
SC30-671185	18:01:47.58	−28:49:04.9	22	557.6±0.6	50.0±6.6	0.332 ±0.068	0.15±0.04	17.4±0.3	1.05
SC32-208566	18:03:22.47	−29:03:43.2	11	690.0±2.0	67.6±20.3	0.577 ±0.296	0.13±0.10	17.3±1.2	0.74
SC33-505	18:05:03.99	−29:18:08.6	14	1778.5±0.4	30.4±6.5	0.466 ±0.153	0.08±0.04	17.1±0.6	0.84
SC33-290665	18:05:29.67	−28:51:03.3	22	1845.3±4.3	73.5±18.9	0.815 ±0.374	0.57±0.50	15.8±1.4	0.73
SC34-606996	17:58:34.18	−29:06:29.4	8	974.9±0.9	154.1±71.0	0.091 ±0.053	0.01±0.00	19.5±0.6	0.72
SC37-556534	17:53:02.92	−30:03:07.8	30	1786.3±0.0	8.3±2.3	0.054 ±0.031	0.05±0.02	17.8±0.4	0.83
SC39-1073	17:55:10.06	−30:10:29.5	24	1807.5±0.2	14.9±3.3	0.563 ±0.205	0.40±0.23	16.3±0.7	0.87
SC39-28566	17:55:10.31	−30:05:11.7	14	1374.0±0.2	21.2±11.4	0.033 ±0.023	0.01±0.01	20.0±0.7	0.75
SC39-54533	17:55:19.53	−29:57:57.0	9	1223.9±2.2	45.6±15.5	0.372 ±0.210	0.05±0.04	17.7±1.3	0.62
SC39-269524	17:55:23.99	−29:55:33.1	11	906.7±0.6	32.2±9.1	0.096 ±0.099	0.03±0.01	16.9±0.5	1.79
SC39-322789	17:55:26.87	−29:43:59.7	12	968.0±0.8	53.2±12.1	0.471 ±0.162	0.10±0.05	16.9±0.6	0.75
SC39-468687	17:55:45.16	−29:56:38.6	10	1210.8±3.7	86.0±22.2	0.572 ±0.256	0.13±0.10	16.8±1.0	0.82
SC39-576039	17:55:43.97	−29:24:28.7	7	620.1±1.1	106.4±40.5	0.360 ±0.188	0.05±0.03	18.1±0.8	1.04
SC39-753576	17:56:01.00	−29:25:11.9	6	1241.2±0.9	88.9±35.8	0.112 ±0.056	0.01±0.00	19.0±0.6	0.79

Note. — The symmetric 68% confidence intervals shown here are only for the purpose of quick reference and avoiding a large amount of unnecessary details. The analysis is based on proper asymmetric confidence intervals. Complete information is available electronically at ApJ web.